Miner Deposita (2008) 43:295–314
DOI 10.1007/s00126-007-0151-5

ARTICLE

Multimillion year thermal history of a porphyry copper deposit: application of U–Pb, $^{40}Ar/^{39}Ar$ and (U–Th)/He chronometers, Bajo de la Alumbrera copper–gold deposit, Argentina

Anthony C. Harris · W. James Dunlap · Peter W. Reiners · Charlotte M. Allen · David R. Cooke · Noel C. White · Ian H. Campbell · Suzanne D. Golding

Received: 17 July 2006 / Accepted: 4 June 2007 / Published online: 16 August 2007

Abstract Application of multiple chronometers (including U–Pb and $^{40}Ar/^{39}Ar$ geochronology and zircon and apatite (U–Th)/He thermochronology) to porphyry intrusions at the Bajo de la Alumbrera porphyry copper–gold deposit, Argentina, reveals a complex history of reheating that spans millions of years. Previous U–Pb geochronology, combined with our new $^{40}Ar/^{39}Ar$ data, shows that the multiple porphyritic intrusions at Bajo de la Alumbrera were emplaced during two episodes, the first at about 8.0 Ma (P2 and associated porphyries) and the second about a million years later (Early and Late P3 porphyries). Complex overprinting alteration events have obscured the earliest hydrothermal history of the deposit. By contrast, $^{40}Ar/^{39}Ar$ data reveal the close temporal relationship of ore-bearing potassic alteration assemblages (7.12±0.13 Ma; biotite) to the emplacement of the P3 intrusions. Consistent with low closure temperatures, younger ages have been determined for associated hydrothermal alkali feldspar (6.82±0.05 Ma and 6.64±0.09 Ma). The temperature-sensitive Ar data also record an unexpected prolonged cooling history (to below 200°C) extending to 5.9 Ma. Our data suggest that the Bajo de la Alumbrera system underwent protracted cooling, after the collapse of the main hydrothermal system, or that one or more low-temperature (~100–200°C) reheating events occurred after emplacement of the porphyritic intrusions at Bajo de la Alumbrera. These have been constrained in part by our new $^{40}Ar/^{39}Ar$ data (including multidomain diffusion modeling) and (U–Th)/He ages. Single-grain (U–Th)/He ages (n=5) for phenocrystic zircon from P2 and P3 intrusive phases bracket these thermal events to between 6.9 (youngest crystallization of intrusion) and 5.1 Ma. Multidomain modeling of alkali feldspar data (from both igneous and hydrothermal crystals) is consistent with the deposit cooling rapidly from magmatic temperatures to below about 300°C, with a more protracted history down to 150°C. We conclude that the late-stage low-temperature (150 to 200°C) thermal

Editorial handling: L. Meinert

Electronic supplementary material The online version of this article (doi: 10.1007/s00126-007-0151-5) contains supplementary material, which is available to authorized users.

A. C. Harris (✉) · D. R. Cooke · N. C. White
CODES ARC Centre of Excellence in Ore Deposits,
University of Tasmania,
7001 Hobart, Australia
e-mail: A.Harris@utas.edu.au

W. J. Dunlap · C. M. Allen · I. H. Campbell
Research School of Earth Sciences,
Australian National University,
2006 Canberra, Australia

P. W. Reiners
Geology and Geophysics Department, Yale University,
New Haven, CT 06520-8109, USA

S. D. Golding
Earth Sciences, School of Physical Sciences,
University of Queensland,
4072 Brisbane, Australia

Present address:
P. W. Reiners
Department of Geosciences, University of Arizona,
Tucson, AZ 85721, USA

anomaly localized at Bajo de la Alumbrera resulted from radiation of heat and/or fluids sourced from deeper-seated magma bodies, emplaced beneath the deposit. To produce the observed thermal longevity of the porphyry system, magma bodies underlying the Bajo de la Alumbrera deposit must have been repeatedly replenished by new magma batches. Without replenishment, crystallization of the source magma will occur, and heat release will stop, leading to rapid cooling (in less than ten thousand years). The influx of deep-seated magma may have caused the development of late low-temperature hydrothermal alteration assemblages at Bajo de la Alumbrera, at the same time that mineralization formed at Agua Rica, some 25 km away. All available chronologic data for the Bajo de la Alumbrera deposit suggest that the hydrothermal system was active episodically over at least a three-million and possibly up to a four-million-year period.

Keywords Porphyry · Copper · Ore-forming fluids · Geochronology · Thermochronology · Longevity

Introduction

The evolution of porphyry ore deposits shows that they result from superposition of multiple magmatic–hydrothermal systems (e.g., Proffett 2003). Alteration assemblages and associated mineralization in porphyry ore deposits develop from huge hydrothermal systems dominated by magmatic and meteoric fluids (Hedenquist and Richards 1998). These systems develop in and adjacent to subvolcanic porphyritic intrusions that are apophyses to deeper-seated magma bodies (Dilles and Einaudi 1992). High-temperature K-silicate alteration develops within and around the intrusions and is interpreted to have been of short duration, whereas low-temperature alteration is longer lived and is believed to migrate inward during thermal collapse of the system (Dilles et al. 2000). A large system of circulating meteoric water is thought to occur on the periphery of the main ore-forming magmatic system (Hedenquist and Richards 1998 and references therein).

Geochronological studies have shown that some phases of multistage subvolcanic porphyry intrusions can have ages distinct from associated magmatic–hydrothermal systems (e.g., Cornejo et al. 1997; Reynolds et al. 1998; Ballard et al. 2001; Gustafson et al. 2001; Harris et al. 2004a; Padilla-Garza et al. 2004; Cannell et al. 2005). It has been shown that the duration of magmatic–hydrothermal activity in some porphyry ore deposits (e.g., Divide, Silberman et al. 1979; Far Southeast-Lepanto, Arribas et al. 1995; Round Mountain, Henry et al. 1995; Potrerillos, Marsh et al. 1997) is approximately equal to or less than the resolution of the K/Ar and $^{40}Ar/^{39}Ar$ techniques. By contrast, a number of porphyry copper systems have associated ages that imply a more prolonged (though likely episodic) duration of formation defined by integration of U–Pb and $^{40}Ar/^{39}Ar$ techniques (e.g., Chuquicamata, Chile, Ballard et al. 2001; El Teniente, Maksaev et al. 2004; Escondida, Chile, Padilla-Garza et al. 2004; Río Blanco, Deckart et al. 2005).

The U–Pb radiometric system in zircon has a closure temperature of more than 900°C. Thus, a U–Pb zircon date effectively gives the crystallization age of the magma from which the zircon crystallized (Lee et al. 1997). Other radioisotopic dating methods, however, do not necessarily measure the age of emplacement of magma; instead, they indicate when the dated minerals cooled through their closure temperatures. This has been well documented for the Ar-based systems; for example, biotite retains Ar below ~300°C (Harrison et al. 1985). Low-temperature thermochronometers, like the (U–Th)/He system, yield ages at which zircon and apatite cooled through temperatures of between ~180 and ~70°C, respectively (Reiners et al. 2004). It is therefore possible to constrain the cooling history of an intrusion and its associated hydrothermal systems if several different techniques are used to date multiple minerals (both igneous and hydrothermal) from one system (e.g., Reynolds et al. 1998; Maksaev et al. 2004; Padilla-Garza et al. 2004; Cannell et al. 2005).

We have applied several chronometers to porphyry intrusions at the Bajo de la Alumbrera porphyry copper–gold deposit, Argentina. The high-temperature (~900°C) history of the system has been determined through U–Pb analysis of zircons. The same decay chain that produces radiogenic Pb in zircon also produces radiogenic He. The significance of the He technique lies in the temperature sensitivity of the age determinations. Our new age determinations (including $^{40}Ar/^{39}Ar$ and (U–Th)/He data), when considered as thermochronometers, suggest that low-temperature thermal events occurred one million years or more after the emplacement of the youngest known porphyritic intrusion. Such findings appear to be inconsistent with numerical simulations of fluid flow around cooling magma bodies, which indicate that heat should dissipate by convection after approximately 100,000 years (Norton and Cathles 1979; Norton 1982).

Regional and ore deposit geology

The Late Miocene Bajo de la Alumbrera copper–gold deposit is one of several porphyry-related ore deposits in the Farallón Negro district (Fig. 1; Sister 1963; Llambías 1972). Magmatism in this region was one of the last events in the evolution of the Miocene magmatic arc of the central Andes (Sasso and Clark 1998). Volcanism in the Farallón

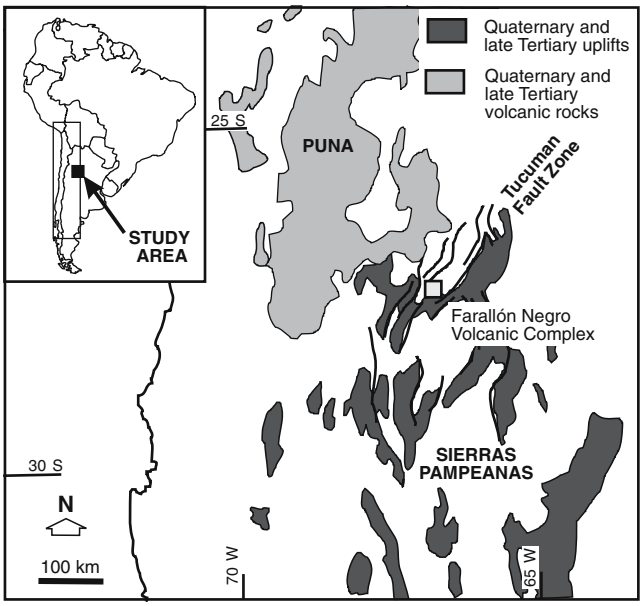

Fig. 1 Physiotectonic map of the central Andes (modified after Ulrich and Heinrich 2002; Proffett 2003) showing the location of the Farallón Negro Volcanic Complex, in which the Bajo de la Alumbrera porphyry copper–gold deposit occurs. The Farallón Negro district is an intermontane basin within a structural deformation zone referred to as the Tucuman Fault Zone. The fault zone marks the transition between the Puna-Altiplano to the north and the Sierras Pampeanas to the south. It is this district that hosts the Bajo de la Alumbrera porphyry ore deposit

Negro Volcanic Complex occurred well inboard (~200 km) of the main magmatic arc during the Late Oligocene and Early Miocene along a crustal scale arc-oblique structural deformation zone, referred to as the Tucuman fault zone (Fig. 1; Sasso and Clark 1998). The Farallón Negro district occurs within the fault zone, which bounds the Puna-Altiplano plateau to the north and the basin-and-range province of the Sierras Pampeanas to the south.

Magmatism in the Farallón Negro district was related to a Miocene orogenic episode that began with the uplift of the Puna-Altiplano (Allmendinger 1986; Sasso and Clark 1998). Crystalline basement that was uplifted during the Middle Miocene became the main source of thick, laterally extensive continental sandstones (e.g., Ramos 1970; Ramos et al. 1998; Kraemer et al. 1999) deposited on a planted basement surface (González Bonorino 1950) and/or in intermontane and foreland basins on the southeastern and southern flank of the Puna-Altiplano (e.g., Bossi et al. 1993; Re 1995; Kraemer et al. 1999). Red-bed sequences thicken westward toward the Precordillera (e.g., Re 1995), which in part reflects the migration of the Puna-Altiplano eastwards, beginning in the Late Oligocene to Early Miocene (Coughlin et al. 1998). The foreland basins were subsequently deformed during a northwest-directed contractional deformation and the progressive easterly translation of the plateau (Jordan and Allmendinger 1986; Jordan et al. 1989; Vandervoort et al. 1995). Cessation of magmatic activity in the Farallón Negro district coincided with Late Miocene–Pliocene uplift of the Sierras Pampeanas (Sasso and Clark 1998; Harris et al. 2004a).

The Farallón Negro Volcanics have a gradational, interfingering relationship with the thick, laterally extensive, red-bed sequences of the El Morterito Formation (Harris et al. 2006). They consist dominantly of sedimentary detritus, with volcanic material derived from small volcanic centers that were once dispersed throughout the district. About 1.5 km (measured thickness) of volcano-sedimentary rock is exposed. These rocks are a heterogeneous mixture of hypabyssal intrusive rocks, lava flows, and flow breccias, phreatomagmatic deposits, reworked pyroclastic deposits, quartz arenite, and debris-flow deposits, representative of a multivent volcanic complex (Proffett 2003; Harris et al. 2006). Intrusive activity occurred throughout the history of the volcanic complex, manifested as subvolcanic dykes, sills, and stocks and syn-sedimentary intrusions (Halter et al. 2004; Harris et al. 2004a, 2006).

As the primary volcanic facies of the Farallón Negro Volcanics are small and laterally discontinuous lava domes (<500 m in diameter) and flows (100–200 m long) extruded from multiple vents, it is likely that the associated magma was sourced from a number of small upper crustal magma bodies (see discussion by Tosdal and Richards 2001). Some magma interacted and assimilated the crust, as implied by the abundant basement-derived inherited zircons in the mineralized porphyries (Harris et al. 2004a). There is also petrological and geochemical evidence that shows magma commingling and/or incomplete mixing was important in the petrogenesis of the Farallon Negro Volcanics (Halter et al. 2004). This includes the occurrence of mafic inclusions in silicic intrusions, sieve textures, and the presence of internal resorption discontinuities in plagioclase (Halter et al. 2004). Cross-cutting relationships combined with U–Pb zircon geochronology show that mineralized porphyritic intrusions were being emplaced in the district at the time that volumetrically more abundant mafic to intermediate magmas were introduced (Harris et al. 2004a).

At Bajo de la Alumbrera, hydrothermal alteration was related temporally and spatially to the emplacement of several plagioclase–biotite (hornblende) phyric dacite porphyries (Fig. 2; Ulrich and Heinrich 2002; Proffett 2003). These intrusions form an intrusive complex approximately 800 m in diameter. The known vertical extent is approximately 1 km and is open at depth. Three broad groups of porphyries define the sequence of intrusive activity, i.e., the plagioclase–phyric dacite P2 porphyries (including the Northeast Porphyry and Los Amarillos Porphyry), biotite–plagioclase–phyric dacite Early P3 porphyries, and the

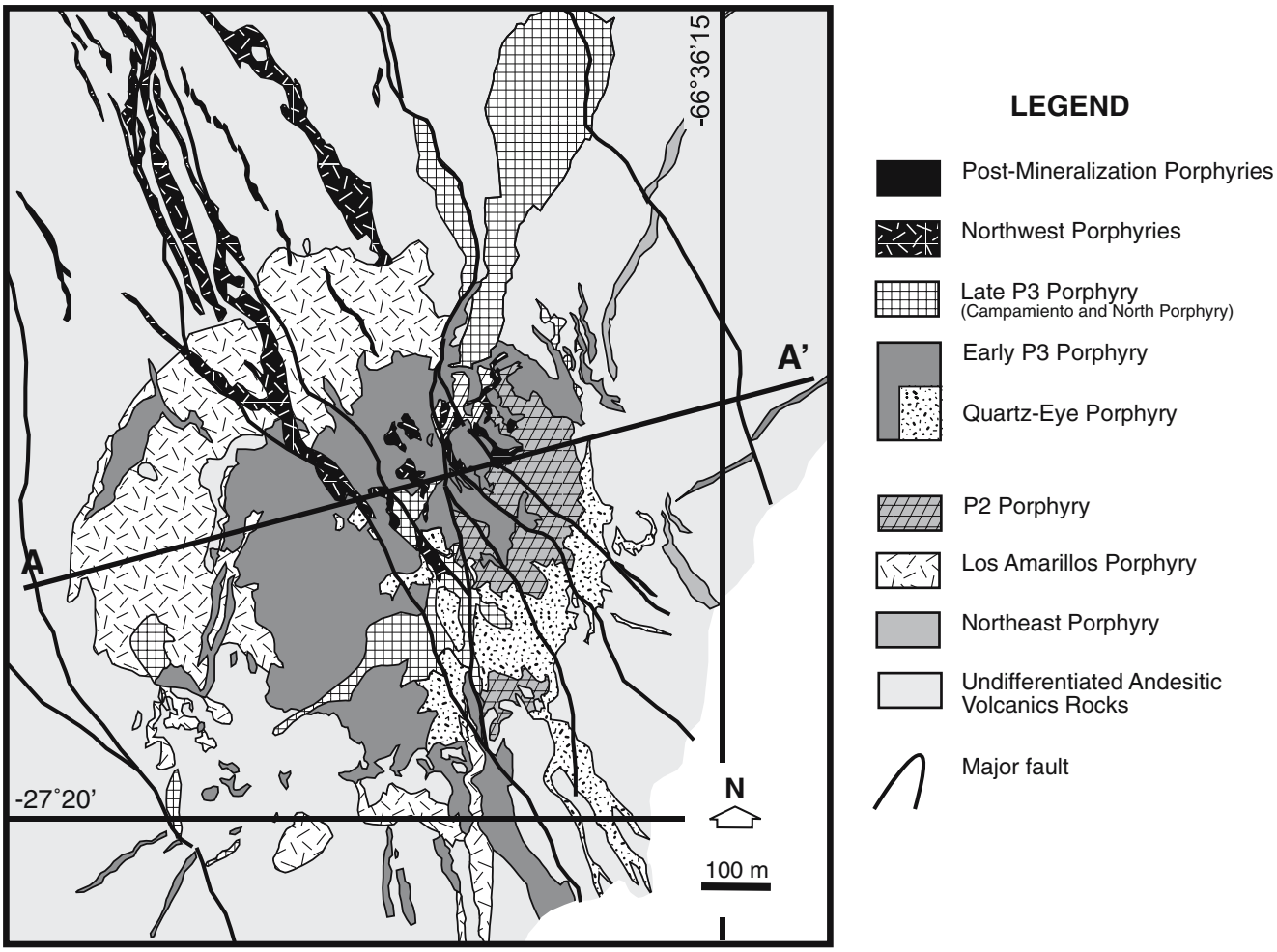

Fig. 2 Simplified geologic map of the Bajo de la Alumbrera deposit (modified after Proffett 2003)

hornblende–plagioclase–phyric dacite Late P3 porphyries. These intrusions are collectively referred to as the "mineralized porphyries" throughout this text. Based on cross-cutting relationships, the youngest known intrusion, emplaced after mineralization, is the Northwest Porphyry (Proffett 2003).

Bajo de la Alumbrera deposit geology

Based on observed cross-cutting relationships, Proffett (2003) interpreted the Northeast Porphyry to be the oldest intrusion at Bajo de la Alumbrera (Fig. 2). The primary igneous mineralogy of this intrusion has been obliterated by a series of texturally destructive hydrothermal alteration events. The oldest intrusion in the deposit that has been dated by radioisotopic techniques is the Los Amarillos Porphyry (Harris et al. 2004a). This intrusion is largely a coherent plagioclase-phyric, biotite- and hornblende-bearing dacite with some brecciated zones. Field relationships show that the P2 Porphyry, another plagioclase-phyric dacite, is younger than the Los Amarillos Porphyry (Proffett 2003).

The Early P3 porphyries (including the Quartz Eye Porphyry) are a group of biotite- and plagioclase-phyric dacites that are volumetrically important (Fig. 2; Proffett 2003). Primary igneous textures are better preserved than in the P2 group of porphyries. Despite being truncated, the Early P3 porphyries appear to rim the subsequent Late P3 porphyries (including the Campamiento and North porphyries). These are a group of hornblende- and plagioclase-phyric dacites containing distinctive euhedral "book" biotites (Proffett 2003; Ulrich and Heinrich 2002; Harris et al. 2004b). One of the last phases of the Late P3 porphyries is coarser grained and more equigranular than the other truly porphyritic phases. Moreover, alkali feldspar phenocrysts are more abundant compared to the other P3 porphyries (Harris et al. 2004b). Despite being petrographically similar to the Late P3 porphyries, the Northwest porphyry and postmineralization dykes are considered on the basis of cross-cutting relationships to be the last intrusive phases in the deposit (Proffett 2003; Ulrich and Heinrich 2002). Paragenesis studies reveal that the copper-gold vein stages cut both the P2 and Early P3 porphyries, with lesser ore found in the Late P3 porphyries (see Fig. 14 of Proffett 2003).

Hydrothermal alteration in the Bajo de la Alumbrera deposit is zoned from a central quartz–magnetite and potassic (biotite–K-feldspar ± quartz–magnetite)-altered core, outward through intermediate argillic (chlorite–illite), phyllic (quartz–muscovite–illite ± pyrite), and propylitic (chlorite–illite–epidote–calcite) assemblages (Fig. 3; Ulrich and Heinrich 2002; Proffett 2003; Harris et al. 2005). At its widest, the most intensely developed and texturally destructive hydrothermal alteration zone is up to 3 km across. The bulk of the copper and gold ore occurs in the potassic alteration zone; however, significant sulfide concentrations are observed in the intermediate argillic and phyllic alteration assemblages (Proffett 2003). K-Feldspar and biotite (with lesser magnetite–quartz) characterize the potassic stages (Proffett 2003). Paragenetic studies show that multiple phyllic events occurred with or without Cu- and Fe-sulfide mineralization (Ulrich et al. 2002; Proffett 2003; Harris et al. 2005). Cross-cutting relationships show that parts of the phyllic assemblages developed before and after the inner Cu–Fe sulfide-bearing intermediated argillic zone (see figure 7 of Harris et al. 2005).

Fluid inclusion microthermometric studies and stable isotope geochemistry have shown that high temperature (up to 850°C) and saline (more than 30 wt% NaCl equivalent) magmatic fluids were responsible for the potassic alteration assemblages (Ulrich et al. 2002; Harris et al. 2005). Lower temperature (from 150 to 300°C) and less saline (<15 wt% NaCl) magmatic fluid and/or admixtures with meteoric water produced the late-stage phyllic assemblages (Ulrich et al. 2002; Harris et al. 2005). Modeling of the isotopic data shows that involvement of meteoric water in the hydrothermal system became important below 200°C (Harris et al. 2005).

Based on measured stratigraphic sections and U–Pb zircon geochronology, it can be demonstrated that the overburden confining the hydrothermal system at Bajo de la Alumbrera has fluctuated through time, with the earliest depths being less than 1 km and growing to greater than or equal to 2.5 km during the main stages of mineralization (Harris et al. 2004a). The maximum thickness is inferred in part from the occurrence of thickly stacked sills and peperitic intrusions in the uppermost portions of the preserved volcano-sedimentary units (Harris et al. 2006). From these estimates, about 1.5 to 2.0 km has been removed from above the current erosion surface. This information may bear on the "low-temperature" thermal excursions, highlighted above and discussed below.

Previous geochronologic studies

A variety of geochronologic data exists for the Farallón Negro district: K/Ar age determinations (Caelles et al. 1971), total fusion and step-heating $^{40}Ar/^{39}Ar$ laser probe ages (Sasso and Clark 1998; Sasso 1997; Halter et al. 2004), and Excimer Laser Ablation inductively coupled plasma mass spectrometry (ELA-ICP-MS) U–Pb zircon age determinations (Harris et al. 2004a). Combined U–Pb zircon (Harris et al. 2004a) and $^{40}Ar/^{39}Ar$ (Sasso 1997; Sasso and Clark 1998; Halter et al. 2004) data indicate that the most voluminous magmatism in the district began as early as 9.5 Ma (as determined by $^{40}Ar/^{39}Ar$) and persisted at least until 6.8 Ma. The U–Pb zircon age data alone indicate that volcanism occurred from 8.46±0.14 to 6.92±0.07 Ma (Harris et al. 2004a). Regional magmatism culminated in the emplacement of rhyodacitic dikes and sills from 6.92±0.07 (U–Pb zircon age: Harris et al. 2004a) to 6.25±0.15 Ma ($^{40}Ar/^{39}Ar$ hornblende age: Halter et al. 2004). Young $^{40}Ar/^{39}Ar$ biotite ages have also been determined for the late felsic intrusions (6.18±0.05 and 6.04±0.07 Ma; ages first reported by Sasso 1997 and subsequently recalculated by Halter et al. 2004).

Emplacement of the multiphased mineralized porphyries occurred not long after magmatism began in the Farallón Negro district: The earliest (P2 Porphyry; Proffett 2003) mineralized porphyries at Bajo de la Alumbrera were emplaced at 8.02±0.14 (U–Pb; Harris et al. 2004a) and 7.98±0.14 Ma (U–Pb; Harris et al. 2004a), whereas late stage (Early and Late P3) porphyries were emplaced about a million years later (7.10±0.07 Ma; U–Pb; Harris et al. 2004a), thus confirming the mapped cross-cutting relationships of Proffett (1997, 2003). In her thesis, Sasso (1997) reported $^{40}Ar/^{39}Ar$ total-fusion and laser step-heating data for mineral separates from a late-stage, postmineralization andesitic porphyritic dike. Ages of 6.78±0.15 and 6.48±0.85 Ma were determined for hornblende and biotite, respectively (Sasso 1997). The biotite ages show poor reproducibility with high atmospheric argon contents (Sasso 1997). Petrographic observations revealed that the biotites are chloritized (as recognized by Ulrich and Heinrich 2002), and therefore recoil effects have possibly disturbed the age (Sasso 1997). Based on this observation, combined with the closure temperature (~500°C) of hornblende, Sasso (1997) interpreted the hornblende $^{40}Ar/^{39}Ar$ age as being the time of crystallization of the Northwest Porphyry.

The timing of hydrothermal alteration at Bajo de la Alumbrera has been constrained previously by total-fusion and laser step-heating $^{40}Ar/^{39}Ar$ ages (data of Sasso 1997 and Sasso and Clark 1998 reinterpreted by Harris et al. 2004a). Sasso and Clark (1998) published several key ages for the deposit. Three biotite $^{40}Ar/^{39}Ar$ ages (7.10±0.13, 6.98±0.08, and 6.83±0.07 Ma), originally interpreted as the age of igneous crystallization (Sasso 1997), were determined from intrusions that occur with and are temporally associated with the potassic alteration zone (which includes secondary biotite). In comparing these ages

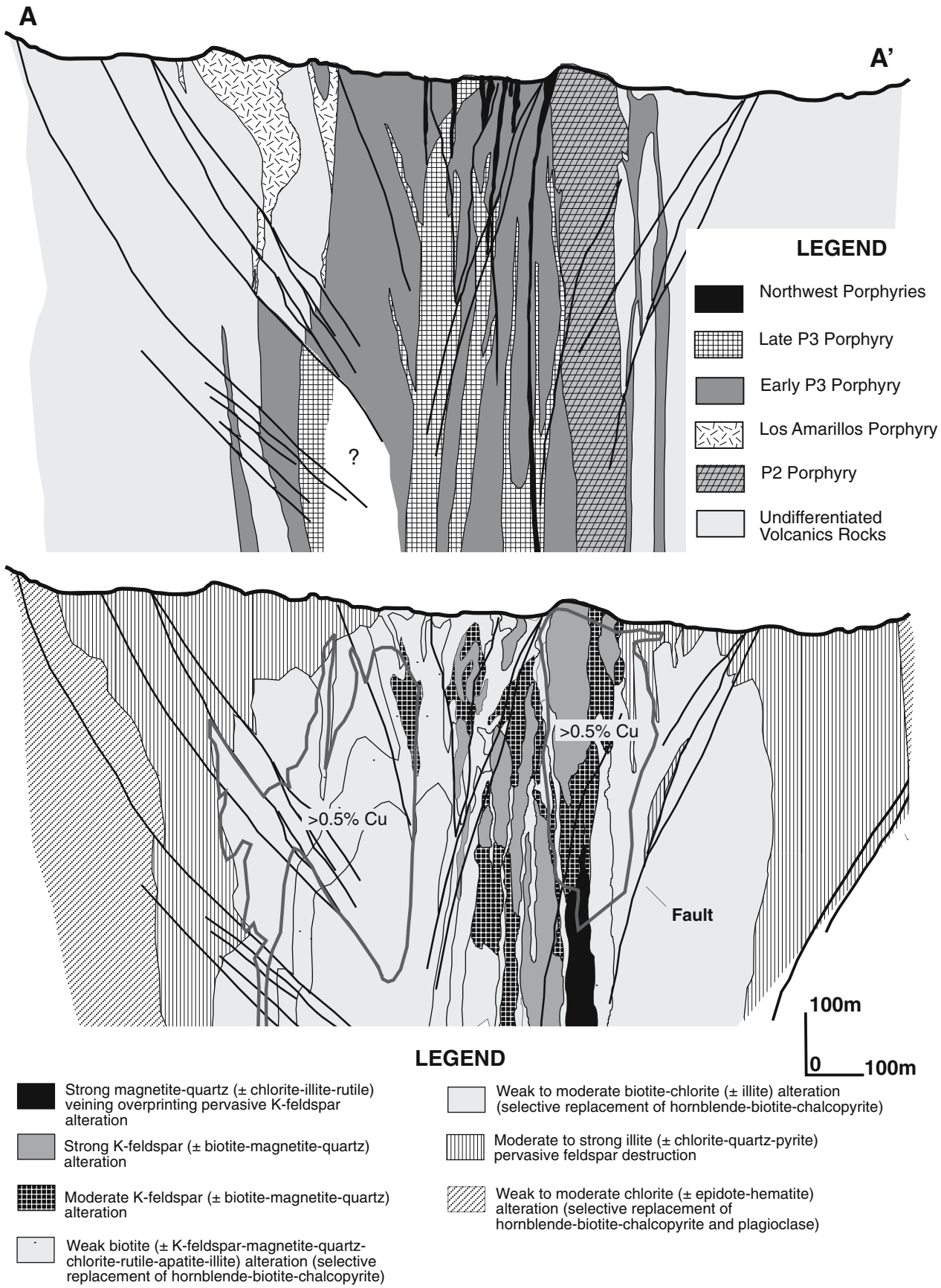

Fig. 3 Simplified geologic cross-section of the Bajo de la Alumbrera deposit (modified after Proffett 2003)

with U–Pb zircon ages of samples from the same porphyry, Harris et al. (2004a) concluded that the $^{40}Ar/^{39}Ar$ ages are not that of primary crystallization. It is more probable that the $^{40}Ar/^{39}Ar$ biotite ages of Sasso and Clark (1998) represent the timing of potassic alteration that overprinted the porphyritic intrusions (Harris et al. 2004a). Sasso and Clark (1998) also reported an $^{40}Ar/^{39}Ar$ age of 6.75± 0.09 Ma (whole rock) for pervasive phyllic alteration, slightly younger than the biotite ages. It may be a mixed age determination, as the whole rock sample is from the innermost zone of pervasive phyllic alteration, which has overprinted intermediate argillic assemblages. In this study, all K-bearing silicate minerals (including those associated with earlier potassic alteration) have been partially or entirely replaced by very fine-grained illite (±chlorite). The potassium concentration (2.81%) of the material analyzed is similar to other whole-rock analyses for the phyllic alteration zone (Ulrich and Heinrich 2002).

Analytical methods

We have applied three different dating techniques to samples of porphyritic intrusions (and the wall rocks that they intruded) from Bajo de la Alumbrera, including U–Pb, $^{40}Ar/^{39}Ar$, and (U–Th)/ He in zircon and apatite. Some of the sample material was used previously in a district-scale ELA-ICP-MS U–Pb zircon study (Table 1 of Harris et al. 2004a). Representative samples include intrusions from the first (i.e., P2 porphyries) and second (i.e., Early and Late P3 porphyries) magmatic stages at Bajo de la Alumbrera. We report (1) a new U–Pb ELA-ICP-MS age for the youngest Late P3 Porphyry (i.e., the last intrusion inferred to be associated with the development of appreciable hydrothermal alteration assemblages at Bajo de la Alumbrera), (2) eight new $^{40}Ar/^{39}Ar$ determinations of phenocrysts and hydrothermal alteration minerals (biotite and alkali feldspar), which provide new insights into the timing of hydrothermal alteration, and (3) ten new (U–Th)/He zircon and apatite ages that constrain the low-temperature history of the deposit (see Electronic Supplementary Material). We also determined (U–Th)/He ages for zircon in the host volcanic rocks (Table 1). These include two volcanic units and the last known subvolcanic intrusion emplaced in the district. Zircon U–Pb ages for these more regional samples have already been described elsewhere (Harris et al. 2004a).

ELA-ICP-MS U–Pb method

U–Th–Pb isotopic compositions of zircons were analyzed at the Australian National University, Canberra, using ELA-ICP-MS. Zircons were separated using conventional heavy liquid separation techniques from rock crushed to pass a 150-μm sieve. The extracted zircons were loosely mounted on double-sided adhesive tape. U–Pb age determinations followed the procedure described by Ballard et al. (2001) and Harris et al. (2004a). Zircons were ablated with a pulsed 193-μm wavelength ArF LambdaPhysik LPX 1201 UV Excimer laser with constant 100 mJ energy, a repetition rate of 5 Hz, and a pit diameter of 29 μm. A mixed Ar–He (with minor H_2) carrier gas transported the ablated material from the sample cell through a flow homogenizer to an Agilent 7500 ICP-MS. Counts for ^{39}Si, ^{96}Zr, ^{31}P, ^{206}Pb, ^{207}Pb, ^{208}Pb, ^{232}Th, and ^{238}U were collected in a time-resolved mode.

The integration times were 50 ms for the three Pb isotopes, 25 ms for U and Th, and 5 ms for all other isotopes, with a total mass sweep time of 0.4 s. Background was measured for 20 s with the laser turned off, and the sample measured for a further 40 s with the laser turned on, giving ~120 mass scans for a penetration depth of ~30 μm. Depth-dependent interelement and isotopic fractionation and instrumental mass bias of Pb, Th, and U (e.g., Hirata and Nesbitt 1995; Horn et al. 2000) were corrected by reference to the standard zircon TEMORA and NIST612 silicate glass (Pearce et al. 1997; Black et al. 2000, 2004). Common Pb (the difference between the measured and expected $^{208}Pb/^{206}Pb$) was then subtracted (Compston et al. 1984), assuming a common Pb composition from the age-dependent Pb model of Cumming and Richards (1975). This showed most analyses to be concordant within analytical uncertainty. Assuming concordance, the $^{206}Pb/^{238}U$ ratios were then calculated by correcting for common Pb. Quoted uncertainties on individual samples are two times the standard uncertainty of corrected $^{206}Pb/^{238}U$ age for the selected portion of the population. Moreover, the U–Pb ages reported here have been corrected for effects of initial isotopic disequilibrium, i.e., ^{230}Th corrected (see Harris et al. 2004a).

$^{40}Ar/^{39}Ar$ method

Alkali feldspar and biotite separates (<250 μm size fraction) used for $^{40}Ar/^{39}Ar$ geochronology were hand picked from mineral separates and rock wafers. A measured amount of mineral separate was wrapped in aluminum foil. The sample and fluence monitors (including the 28.1-Ma Fish Canyon Tuff sanidine standard 92–176) were then sealed in an aluminum canister containing an inner tube of silica glass wrapped in a 0.2-mm-thick cadmium liner. The canister was irradiated for 24 h in the HIFAR reactor at Lucas Heights, New South Wales. During that time, the canister was inverted three times to reduce the neutron fluence gradient across the container (Spell and McDougall 2003). Correction factors to account for K-, Cl-, and Ca-derived Ar isotopes are $(^{36}Ar/^{37}Ar)_{Ca}=3.5\times10^{-4}$, $(^{39}Ar/^{37}Ar)_{Ca}=7.86\times$

Table 1 Description of samples used for age determinations

Sample	Location	Description
Bajo de la Alumbrera Hydrothermal		
ACH-99166	DDH48.5–54 139 m	P2 Porphyry altered to K-feldspar–biotite–magnetite–quartz. Intense pervasive biotite–magnetite alteration obscures phenocrysts and groundmass mineralogy. Biotite phenocrysts are recrystallized and the groundmass feldspars are altered to a mosaic of biotite–quartz–K-feldspar ± chlorite–rutile–apatite. Quartz ± chalcopyrite–K-feldspar veins cut this pervasive alteration. $^{40}Ar/^{39}Ar$ age determined for hydrothermal biotite.
ACH-9985	DDH50.46.43 613.2 m	Early P3 Porphyry altered to K-feldspar–biotite. Plagioclase phenocrysts are largely replaced by K-feldspar. Irregular patches of ragged biotite have replaced the groundmass. Biotite from this pervasive alteration was separated for $^{40}Ar/^{39}Ar$ age determination.
ACH-9980	DDH50.46.45 726.5 m	Early P3 Porphyry. Early P3 Porphyry cut by magnetite–quartz–chalcopyrite veins. Pervasive K-feldspar (±biotite) and magnetite alters the groundmass. Clusters of coarse hydrothermal alkali feldspar were hand picked for $^{40}Ar/^{39}Ar$ age determination.
ACH-9984	DDH49–50.1, 75 m	Early P3 Porphyry altered to K-feldspar–biotite ± quartz–magnetite. Intense pervasive K-feldspar–biotite–quartz ± chalcopyrite–magnetite has obliterated the groundmass. Diffuse quartz–chalcopyrite veins cut this potassic alteration assemblage. Plagioclase phenocrysts are altered to illite ± chlorite. Patches of the groundmass are also altered by chlorite. Rare pyrite veins cut all alteration stages. The least-altered hydrothermal biotite was hand picked for age determination.
ACH-99155	DDH 50.4–64.3 625.5 m	Late P3 Porphyry. Pervasive biotite–magnetite alteration obscures phenocrysts and groundmass. Biotite phenocrysts are recrystallized and the groundmass feldspars are altered to a mosaic of biotite–quartz–K-feldspar ± chlorite–rutile–apatite. Chlorite ± illite alteration affects the biotite phenocrysts and less commonly the secondary biotite. Sample overprinted by intense pervasive illite–chlorite alteration. Illite–chlorite assemblages replace large feldspars.
Igneous		
ACH-9998	DDH 49.2–64.3 770.9 m	Late P3 Porphyry [Bt (<3 mm; <5%), Hbl (<5 mm; <3%), Plag (<5 mm; <25%), Qtz (<2 mm; <10%), alkali feldspar (<2 mm; <2%)]. Alkali feldspar phenocrysts are anhedral, subhedral to euhedral, and occur in some phases of the Late P3 Porphyry. The aphanitic groundmass comprises quartz and feldspar. Small anhedral to subhedral apatite and zircon crystals are dispersed through the groundmass. Sample lack pervasive alteration assemblages. Rare magnetite veins. U–Pb (zircon) and $^{40}Ar/^{39}Ar$ (alkali feldspar and biotite) age determinations were undertaken on unaltered phenocrysts. (U–Th)/He analyses were undertaken on zircon and apatite.
ACH-99158	DDH47–64.3 831.2 m	Late P3 Porphyry [Bt (<3 mm; <5%), Hbl (<5 mm; <3%), Plag (<5 mm; <25%), Qtz (<2 mm; <10%), Alkali feldspar (<2 mm; <2%)]. Little to no hydrothermal alteration assemblages. Pristine igneous biotite was used for $^{40}Ar/^{39}Ar$ age determination.
ACH-9981	DDH47–64.3 786.5 m	Relatively fresh Late P3 Porphyry, with large (up to 8 mm) biotite phenocrysts [Bt (<3 mm; <5%), Hbl (<5 mm; <3%), Plag (<5 mm; <25%), Qtz (<2 mm; <10%), alkali feldspar (<2 mm; <2%)]. Although rarely seen, this biotite is locally replaced by chlorite. Associated with the chloritized biotite are veinlets of pyrite. Ages were determined for the least altered biotite phenocrysts.
ACH-9923	−66°36′19.4 −27°19′56.1	Los Amarillos Porphyry (P2). [Hbl (2–3 mm, <2%), Bt (<5 mm, <5%), Plag (1–5 mm, <30%), Qtz (<5 mm, <15%). K-feldspar–quartz ± magnetite altered P2 Porphyry cut by quartz ± chalcopyrite ± magnetite veinlets. Clots of chlorite–illite ± quartz have replaced the groundmass. Chalcopyrite–pyrite veins (with chlorite–illite alteration selvage) cut the porphyry. Illite–pyrite–chalcopyrite veins cut all early alteration assemblages. Zircon separates were used for (U–Th)/He age determination.
ACH-1084	−66°35′53.8 −27°20′5.5	Late P3 Porphyry [Bt (<5 mm; <5%), Hbl (<3 mm; <3%), Plag (<5 mm; <25%), Alkali feldspar (<2mm; trace)]. Zircon separates from earlier U–Pb dating (Harris et al. 2004a) were used for (U–Th)/He age determination.
ACH-P2	DDH49–60 182 m	P2 Porphyry [Hbl (2–3 mm, <2%), Bt (<5 mm, <5%), Plag (1–5 mm, <30%), Qtz (<5 mm, <15%). Intense illite alteration of plagioclase. Biotite altered by chlorite. Stockwork of veinlets of quartz–chalcopyrite ± biotite–K-feldspar. Stringers of chalcopyrite very abundant. U–Pb zircon age published previously (Harris et al. 2004a). (U–Th)/He analyses were determined for residual zircons from original study.
Regional		
ACH-00245	−66°37′49.7 −27°15′53.9	Plag (2–4 mm, 5–10%); Cpx (<5 mm; <15%). No hydrothermal alteration assemblages
ACH-1063	−66°42′24.9 −27°16′55.1	Bt (<5 mm, <5%), Hbl (<2 mm, <2%), Plag (1–5 mm, <30%), Qtz (<5 mm, <10%). Unaltered
ACH-1065	−66°42′36.8 −27°15′17.4	Hbl (2–3 mm, <5%), Bt (<5 mm, <2%), Plag (<10 mm, <15%) Kflds (<40 mm, <2%) [Macho Muerto Rhyodacite]. Unaltered

Percentages are averages of visual estimates of volume percent in thin sections and cut slabs; grain sizes refer to long dimensions.
Bt Biotite, *Cpx* clinopyroxene, *Hbl* hornblende, *Kflds* K-feldspar, *Plag* plagioclase, *Qtz* quartz, *N.D.* not defined

10^{-4}, $(^{40}Ar/^{39}Ar)_K = 7.0 \times 10^{-2}$, $(^{38}Ar/^{39}Ar)_K = 0.136$, $(^{38}Ar)_{Cl}/(^{39}Ar)_K = 8.0$.

The irradiated mineral separates were loaded onto an extraction line connected to a VG 3600 gas source mass spectrometer, with a sensitivity of $\sim 3 \times 10^{-17}$ mol mV^{-1}. Unknown samples were heated in a low-blank resistance furnace in a series of steps for variable durations. Data were reduced using the Macintosh program "Noble," developed at the Research School of Earth Sciences. The $^{40}Ar/^{39}Ar$ ages reported here are based on reference to the 28.1-Ma Fish Canyon Tuff sanidine standard (92–176). This standard generally has less than 0.3% uncertainty in determining the *J* value of irradiation (Spell and McDougall 2003). Blanks and backgrounds were generally atmospheric and/or insignificant in terms of fraction of the gas analyzed. Air standards were used to determine mass fractionation, which is known within about 0.3%, and was assumed not to vary on the time scale of sample analysis.

As this study integrates two different geochronometers, factors affecting cross-calibration of $^{40}Ar/^{39}Ar$ geochronology with the results of more precise U–Pb analyses need to be considered. Uncertainties in the decay constant values inhibit accurate cross-calibration, as the ages determined are apparent ages relative to the known standards (Renne et al. 1998; Villeneuve et al. 2000). However, this is a problem when dating rocks hundreds of millions of years old, not the millions-of-years-old rock like those being considered in this study (Villeneuve et al. 2000). Lanphere and Baadsgaard (2001) have shown that for young material, there is good agreement within analytical uncertainty between $^{40}Ar/^{39}Ar$ and U–Pb analyses. Based on these studies, we believe that the cross-calibration effect between the U–Pb and Ar technique is negligible, and it is not considered further.

(U–Th)/He method

Single-grain apatite and zircon (U–Th)/He age determinations were performed at Yale University by neodymium-doped yttrium–aluminium–garnet (Nd YAG) laser heating to extract helium and sector ICP-MS to measure U and Th, according to the procedures of Reiners et al. (2004). Euhedral mineral grains were hand picked from separates prepared from 1-kg samples using conventional magnetic and heavy liquid separation techniques. Individual zircons and apatites were loaded into 1-mm Pt (apatite) or Nb (zircon) foil tubes and placed in copper or stainless steel sample planchets. The planchets were loaded into a laser cell, and once under vacuum, the foil tubes were individually heated by a Nd YAG laser for 3 min for apatites and 20 min for zircons. Individual grains were reheated to check for quantitative He degassing. ^4He blanks were determined by heating empty foil tubes using the same procedure. The liberated gas was spiked with ^3He and purified through freezing down of volatiles onto a charcoal trap. $^4He/^3He$ ratios were measured on a quadrupole mass spectrometer. All ratios were referenced to multiple same-day measured ratios and known volumes of ^4He standards. Standard reproducibility averages 0.2% on a daily and long-term basis. The estimated 2σ analytical uncertainty on He determinations is 2–4%.

Once retrieved from the laser cell, the zircons were spiked with a calibrated ^{229}Th and ^{233}U solution and dissolved at pressure using mixed acid digestion. Apatites (in Pt tubes) were dissolved in HNO_3-filled Teflon tubes, whereas zircons and the enclosing Nb foils were dissolved in Teflon microvials in Parr bombs filled with HF and HNO_3. A precipitate was formed and then collected and subsequently dissolved in HCl. The residual precipitate was then dissolved in HNO_3. The spiked solutions were analyzed on a Finnigan Element2 ICP-MS. Routine in-run precision and long-term reproducibility of standard $^{232}Th/^{229}Th$ and $^{238}U/^{233}U$ is 0.1–0.4%, and the uncertainty on measured U–Th concentrations is 1–2% (2σ). Alpha ejection was corrected using the method of Farley et al. (1996), Farley (2002), and Hourigan et al. (2005). Based on the repeat analysis of Fish Canyon Tuff zircons and other in-house standards, analytical uncertainty for the single-grain zircon and apatite age determinations are estimated at 8 and 6% (2σ), respectively.

Several studies have shown the temperature sensitivity (i.e., low-closure temperature) of the (U–Th)/He technique compared to $^{40}Ar/^{39}Ar$ ages for coexisting minerals, including alkali feldspar (Reiners et al. 2002, 2003). These interchronometer calibrations highlight that zircon He ages typically agree (within 1σ) with the alkali feldspar $^{40}Ar/^{39}Ar$ multidomain cooling modeling (Reiners et al. 2004). Such studies also constrain the (U–Th)/He closure temperatures to ~180°C for zircon and ~70°C for apatite.

Geochronologic and thermochronologic results

U–Pb systematics

$^{206}Pb/^{238}U$ zircon ages for the main porphyries at Bajo de la Alumbrera have been reported (Table 1). Harris et al. (2004a) determined ages of 8.02±0.14 and 7.98±0.14 Ma for the Los Amarillos and P2 porphyries, respectively. By contrast, zircons from two samples of the P3 group of porphyries (both Early and Late P3) returned ages of 7.10±0.07 Ma. We report a new $^{206}Pb/^{238}U$ age for sample ACH9998, from the youngest Late P3 phase; i.e., that least affected by pervasive hydrothermal alteration. This sample was collected from the deepest drill hole at Bajo de la Alumbrera (diamond drill hole 49.64.3 sampled at

770.9 m). It differs from other Late P3 phases in being coarser grained and typically equigranular. Megacrysts of alkali feldspar (<12.0 mm; <5% mode) occur as subhedral- and euhedral-twinned clusters. Myrmekitic intergrowths define concentric zonation (or resorption features) within the alkali feldspar (Harris et al. 2004b). Like other Late P3 porphyries, this phase is rich in hornblende and biotite. Biotite (<3.0 mm; <5% mode) phenocrysts occur as distinct "books," while hornblende (<5 mm; <3% mode) occurs as euhedral crystals. Plagioclase (<5 mm; <25% mode) occurs as euhedral oscillatory-zoned crystals and as euhedral-twinned clusters. Quartz eyes are more abundant than in most Late P3 porphyries and are equant bipyramidal crystals. The groundmass comprises quartz and feldspar. Small anhedral to subhedral apatite and zircon crystals are dispersed through the groundmass and also occur as clusters in feldspar phenocrysts.

We have determined an age of 6.96±0.09 Ma for sample ACH9998 zircon, based on 24 grains (Table 2 Electronic Supplementary Material; Fig. 4). Individual zircons used in this age determination have mean ages ranging from 6.2 to 7.3 Ma. Another 13 analyses were excluded from the final age determination based on the criteria listed by Harris et al. (2004a). This $^{206}Pb/^{238}U$ age is indistinguishable from the U–Pb age of the last known subvolcanic intrusion emplaced in the Farallón Negro district, i.e., 6.86±0.05 Ma for the Macho Muerto Rhyodacite (Harris et al. 2004a). Moreover, this age is indistinguishable from ages of intrusions found in subeconomic porphyry Cu deposits that surround Bajo de la Alumbrera (e.g., Bajo el Durazno and las Pampitas; see Harris et al. 2004a). Our new ELA-ICP-MS zircon U–Pb geochronology is consistent with the observed cross-cutting relationships. A subset of subtly inherited ~8.0-Ma zircons appears to have been derived from the older group of P2 porphyries. Unlike other mineralized porphyries, particularly the P2 Porphyry, no basement-derived inherited zircons were found in the last known porphyritic intrusion at Bajo de la Alumbrera.

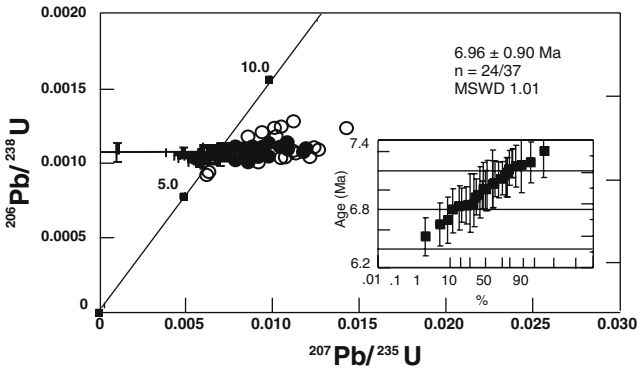

Fig. 4 Concordia plot and probability plots of ELA-ICP-MS U–Pb results used in calculating the $^{206}Pb/^{238}U$ zircon age of sample ACH9998 from the Bajo de la Alumbrera deposit. On the Concordia portion: the uncorrected data are *circles*, where the *filled circles* are the selected data used for the final age calculation. *Open circles* are data omitted from the final age calculation (using criteria defined in Harris et al. 2004a, b). *Crosses* are data both ^{208}Pb and ^{230}Th corrected with 2σ uncertainties including uncertainties in standards. On the smaller probability diagram, all ^{208}Pb- and ^{230}Th-corrected data are plotted as *squares*, with the data omitted on the probability plot basis shown as the *open symbols*. These U–Pb analyses have revealed zircon inheritance. One group of older zircons in the late P3 porphyries have ages of about 8.0 Ma and are interpreted as being sourced from older mineralized and altered porphyritic intrusions (e.g., P2 group of porphyries). A second group of inherited zircons are only slightly older than the mean age (i.e., up to 7.3 Ma of the intrusion)

$^{40}Ar/^{39}Ar$ systematics

Hydrothermal minerals We have determined four new incremental heating $^{40}Ar/^{39}Ar$ age spectra for hydrothermal biotite and K-feldspar that have altered both P2 and Early P3 porphyries. Figures 5 and 6 show the age spectra for the hydrothermal biotites and alkali feldspars. Figure 7 shows the Cl/K and K/Ca ratios vs percent ^{39}Ar release in addition to the laboratory age spectra for alkali feldspars. All Ar isotopic data are presented in Tables 3 and 4 (Electronic Supplementary Material). Ages quoted for each sample are derived from the plateau or plateau-like segment of the age spectrum.

The age spectrum for sample ACH99166 hydrothermal biotite (Fig. 5) comes from an alteration assemblage overprinting P2 Porphyry. The biotite is found in selvages of quartz–chalcopyrite veins. Typically, the biotite occurs as fine (<150 μm)-ragged clots that have replaced the igneous groundmass. Micron-scale chlorite intergrowths occur along the biotite cleavage. Only the least altered grains were hand picked and selected for analysis. This biotite yields a somewhat nonuniform degassing spectrum, which in part defines a plateau-like segment. Excluding the first portion of ^{39}Ar release, which appears contaminated by absorbed atmospheric argon, the apparent ages increase from 6.39±0.69 to 7.82±0.48 Ma. After about 45% of ^{39}Ar release, the apparent ages (and their uncertainties) cluster between 7.6 and 6.5 Ma. The total fusion age of this secondary biotite separate is 7.08±0.95 Ma, which is considerably younger but within analytical uncertainty of the $^{206}Pb/^{238}U$ zircon age (7.98±0.14 Ma) of the P2 Porphyry. Based on a large portion of ^{39}Ar gas release (approximately 30%), a poor plateau-like segment defines an age of 7.22±0.18 Ma. Like the total fusion age, this preferred age is within uncertainty of those of the younger P3 porphyries. Moreover recrystallization and/or replacement of the biotite by later high-temperature (in excess of 300°C) hydrothermal fluids (related to the P3 porphyries) could have caused partial outgassing of accumulated argon.

A new $^{40}Ar/^{39}Ar$ age determination has been made for hydrothermal biotite from an Early P3 Porphyry (Fig. 5, sample ACH9985). Irregular patches of fine-grained ragged biotite have replaced the igneous groundmass. Unlike the

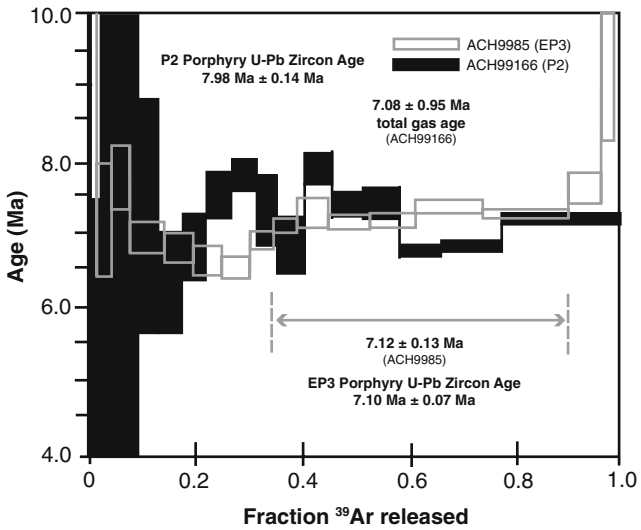

Fig. 5 Age spectra determined for hydrothermal biotite from the P2 and Early P3 Porphyry (Sample ACH99166 and ACH9985, respectively). Sample ACH99166 yields a total fusion age of 7.08±0.95 Ma, which is within analytical uncertainty of the $^{206}Pb/^{238}U$ zircon age (7.98±0.14 Ma) of the P2 Porphyry. The best age of the sample (based on approximately 30% of ^{39}Ar release) is 7.22±0.18 Ma (1σ), which is within uncertainty of the younger P3 porphyries. Given the fine-grained nature of the material being analyzed, the possibility of argon loss cannot be excluded. By contrast, a more systematic and uniform release spectrum has been determined for secondary biotite associated with P3 (ACH9985). Although the presence of excess ^{40}Ar cannot be excluded, the calculated 7.12±0.13-Ma plateau age of the hydrothermal biotite is within analytical uncertainty (2σ) of the $^{206}Pb/^{238}U$ zircon age (7.10±0.07 Ma) of the associated intrusion

secondary biotite analyzed from the P2 porphyry, the ACH9985 hydrothermal biotite from a younger porphyry phase yields more systematic Ar degassing. After the first fraction of ^{39}Ar release, the apparent ages decline (to 6.63± 0.19 Ma) before rising to a plateau of six contiguous segments and 45% of the total Ar release (Fig. 5). Although the presence of excess ^{40}Ar cannot be excluded, the calculated plateau age (7.12±0.13 Ma) of the hydrothermal biotite is within analytical uncertainty of the $^{206}Pb/^{238}U$ zircon age (7.10±0.07 Ma) of the Early P3 Porphyry wall rock. Further, this new hydrothermal biotite age is within analytical uncertainty of two of three biotite $^{40}Ar/^{39}Ar$ ages (namely, 7.10±0.13 and 6.98±0.08 Ma) previously reported for intrusions at Bajo de la Alumbrera (Sasso 1997; Sasso and Clark 1998).

Two multistepped incremental heating ages have been established for hydrothermal alkali feldspar overprinting the Early P3 Porphyry (Fig. 6). Feldspars with contrasting alteration histories and intensities have been analyzed. Sample ACH9980 represents a relatively simple alteration assemblage of near-total replacement of the igneous groundmass by alkali feldspar. In contrast, feldspar-separate ACH9984 is derived from a complex assemblage of alkali feldspar–biotite–quartz ± chalcopyrite–magnetite that has largely obliterated the Early P3 groundmass. Both alkali feldspar concentrates yield age spectra that record a complex history. In both samples, the lowest temperature steps (up to 650°C) show presence of excess ^{40}Ar or are dominated by atmospheric argon related to the cracking and venting of fluid inclusions during heating. After this initial degassing, the apparent ages decrease to between 5.9 and 6.3 Ma before rising again to much older apparent ages. Melting of the alkali feldspar occurred at temperatures above 1,140°C. Integrated ages of 6.64±0.09 and 6.82± 0.05 Ma have been calculated for sample ACH9980 and ACH9984, respectively. These integrated ages of the alkali feldspar are younger than the U–Pb zircon age of the porphyry they alter (i.e., 7.10±0.07 Ma for the Early P3 Porphyry), but the older ages in the two spectra contradict the U–Pb data and are difficult to explain; trapped large domain excess argon could be the cause (Foster et al. 1990).

Igneous minerals We have also undertaken new $^{40}Ar/^{39}Ar$ age determinations for phenocrystic alkali feldspar and biotite from the Late P3 Porphyry. Cross-cutting relationships are helpful in confirming that the Late P3 porphyries are largely unaltered. These are considered to postdate the bulk of the mineralization. Significant metal accumulation occurs around the Late P3 group of porphyries (see Proffett 2003). Figure 7 shows the age spectra for the phenocrystic biotites from the Late P3 Porphyry. Figure 8 shows the Cl/K and K/Ca ratios vs percent ^{39}Ar release diagram, as well as the age spectra for the two alkali feldspars. All Ar isotopic data for the phenocrysts are presented in Tables 3 and 4 (Electronic Supplemetary Material).

Biotite from sample ACH99158 yields a simple degassing spectrum (Fig. 7). The total gas age of this sample is 7.19±0.33 Ma. The three lowest and the two highest temperature steps were omitted to determine our preferred age, as they show the presence of excess ^{40}Ar or are dominated by atmospheric argon. Based on seven contiguous steps and approximately 54% of the ^{39}Ar, the preferred age of this phenocrytic biotite is 7.15±0.1 Ma, which is within analytical uncertainty of the $^{206}Pb/^{238}U$ zircon age of the P3 group of porphyries (7.10±0.07 and 6.96±0.09 Ma).

Despite being apparently unaltered, biotite phenocrysts from ACH9998 yield disturbed age spectrum, with non-uniform Ar degassing generating a distinct peak when 30 to 40% of the ^{39}Ar had been released (Fig. 7). A plateau of three or more contiguous steps was not defined because of the release of contaminating volatiles (age peak) upon dehydroxylation at around 700–800°C (e.g., Dunlap and Kronenburg 2001). The total gas age of the biotite separate is 7.73±0.19 Ma. This age is older than the $^{206}Pb/^{238}U$ zircon age (6.96±0.09 Ma) of the rock and implies excess

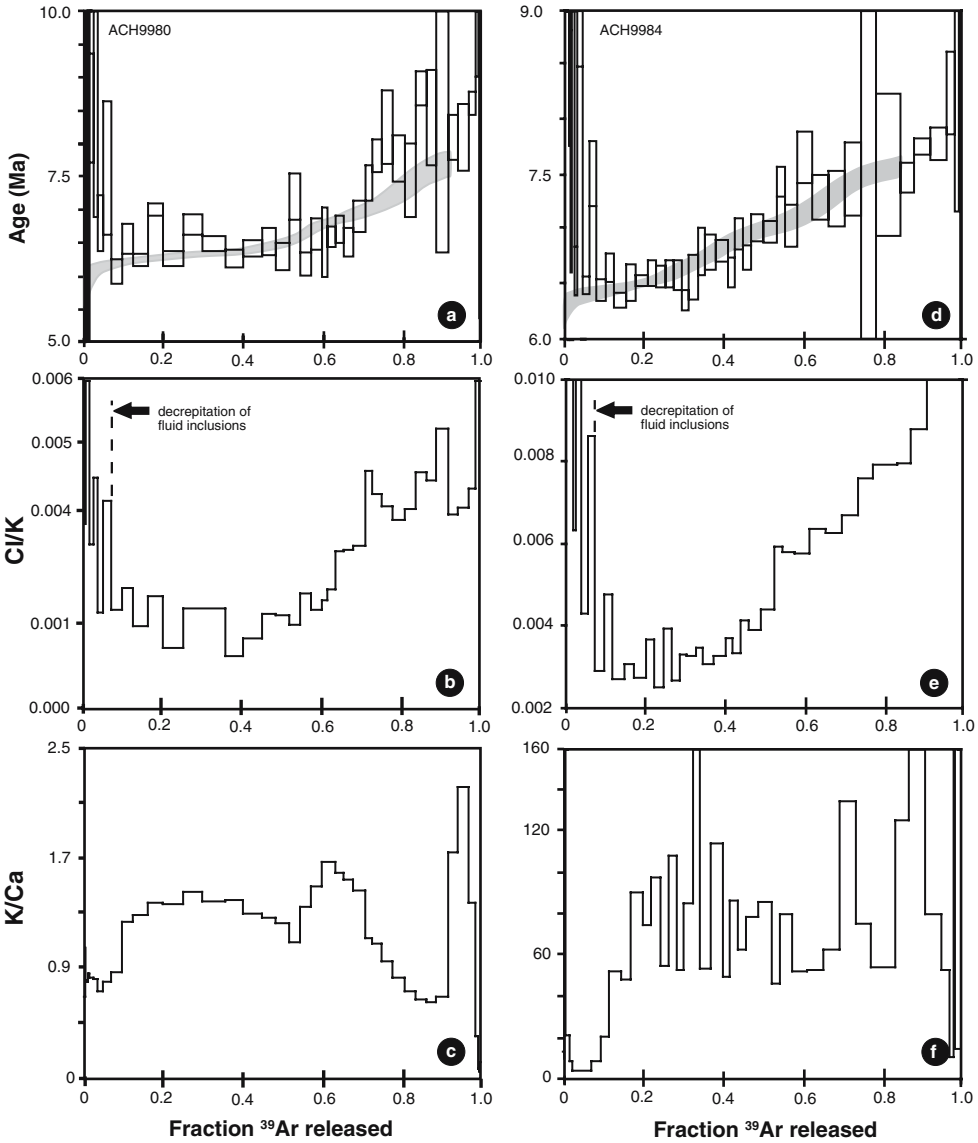

Fig. 6 **a**, **d** Laboratory-derived $^{40}Ar/^{39}Ar$ age spectrum for hydrothermal alkali feldspar from Early P3 Porphyry (Sample a ACH9980 and d ACH9984). Included is the multidiffusion domain model age spectrum (*gray fill*). Note that model rises monotonically with increasing gas release (from *left* to *right*). **b**, **e** Calculated Cl/K ratios and **c**, **f** K/Ca ratios vs fraction of ^{39}Ar released for the alkali feldspar. See text for discussion

argon in the biotite, confirming the conclusions of Dunlap and Kronenburg (2001).

Age spectra for ACH9998 and ACH9981 (phenocrystic alkali feldspar) are complex (Fig. 8). Sample ACH9998 is characterized by high initial ages, which decrease to ages between 6.3 and 6.1 Ma before rising to maximum ages of ~7.5 Ma. Similarly, sample ACH9981 is characterized by geologically meaningless initial ages, which decrease to ages between 6.6 and 5.9 Ma before rising again after about 40% of ^{39}Ar released. The apparent ages determined during the bulk of the gas release range from 7.2 to 9.1 Ma. We explain these spectra patterns, not in terms of excess argon, but in terms of an apparent Ar diffusion from essentially homogeneous alkali feldspar. The first 5 to 10% of gas release at low-temperature heating gave geologically meaningless ages. Heating of the mineral separates to about 650°C produced decrepitation of primary fluid inclusions in the mineral separates. Evidence for the cracking and release of fluid inclusion Cl during this initial heating is provided by the highly elevated Cl/K ratios in the initial release (Fig. 8b). In the case of alkali feldspar from sample ACH9998, subsequent gas release yielded systematically increasing ages from 6.1 to 7.5 Ma. After about 45% of ^{39}Ar released, the evolved ages become nearly constant.

(U–Th)/He thermochronology

Table 5 summarizes the single-grain zircon and apatite (U–Th)/He age determinations (see Electronic Supplementary Material). Of the five samples analyzed, the three regional (up to 8 km away from Bajo de la Alumbrera) samples have zircon He ages that are concordant (within analytical

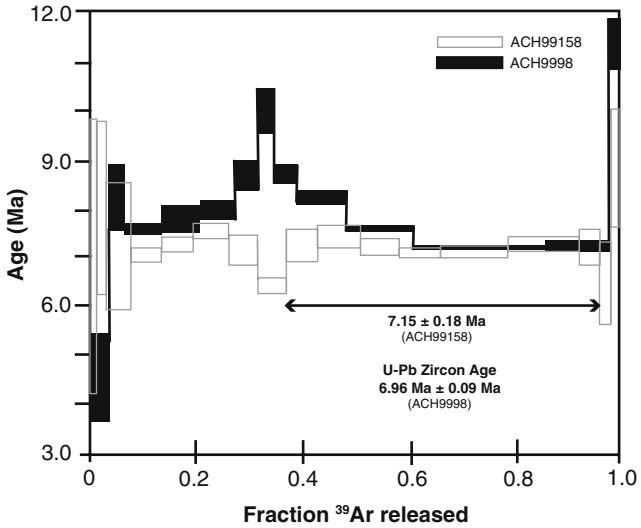

Fig. 7 Age spectra determined for biotite phenocrysts from Late P3 Porphyry (Sample ACH9998 and ACH99158). Sample ACH9998 spectrum is disturbed, yielding a nonuniform release spectrum characterized by a distinct peak between 30 and 40% of ^{39}Ar released. Based on the known zircon age, we interpret that the biotite has been recrystallized during reheating by a thermal event that did not exceed 300°C for a protracted period of time. A more uniform spectrum has been determined for another phenocrystic sample in the same intrusive phase. Based on seven contiguous steps and approximately 54% of the Ar degassing, the preferred age of this phenocrytic biotite is 7.15± 0.18 Ma, which is within analytical uncertainty (2σ) of the ^{206}Pb/^{238}U zircon age of the P3 group of porphyries (7.10±0.07 and 6.96± 0.09 Ma) porphyries

uncertainty at the $\pm1\sigma$ level) with the U–Pb zircon ages. For example, the zircon from a lava unit at the base of the volcanic sequence has a zircon He age of 8.31±0.33 Ma (Table 5, ESM) that is within uncertainty of the U–Pb zircon age (8.42±0.10 Ma; Harris et al. 2004a). Similarly, the youngest known subvolcanic intrusion in the Farallón Negro Volcanic Complex (i.e., the Macho Muerto Rhyodacite) has a U–Pb zircon age of 6.86±0.05 Ma (Harris et al. 2004a) that is concordant to the zircon He age 6.60± 0.27 Ma for the same sample. The available ^{40}Ar/^{39}Ar ages (Sasso 1997; Sasso and Clark 1998; Halter et al. 2004) for this intrusion are also within analytical uncertainty of this new zircon He age.

In contrast to the above samples, the (U–Th)/He ages from zircons in mineralized porphyritic intrusions at Bajo de la Alumbrera are younger than the magmatic U–Pb zircon age. For example, P2 (sample ACHP2), with a U–Pb of 8.02±0.14 Ma, yields a single-grain zircon He age of 5.83±0.24 Ma. Another P2 porphyry (sample ACH9923) has ^{206}Pb/^{238}U zircon and zircon He ages of 7.98±0.14 and 6.07±0.12 Ma, respectively. Both of these porphyry samples come from the uppermost parts (<300 m from current topography) of the Bajo de la Alumbrera deposit. Similar, though less extreme, differences are found in U–Pb and (U–Th)/He ages of the younger (~7.0 Ma) porphyry phases. An altered example of the Late P3 Porphyry (sample ACH99155) yields a zircon U–Pb age of 7.10± 0.07 Ma and a zircon He age of 6.55±0.26 Ma. Sample ACH99155 was taken from the base of economic mineralization at Bajo de la Alumbrera, several hundred meters below the present-day surface. An unaltered example of the Late P3 Porphyry, similarly from the base of economic mineralization, has U–Pb and zircon He ages of 6.96±0.09 (this study) and 5.21±0.10 Ma, respectively (ACH9998). A surface sample of the Late P3 Porphyry (ACH1084), found in the outermost zones of hydrothermal alteration (between potassic and propylitic assemblages), has a magmatic age of 7.10±0.07 Ma, compared to a single-grain zircon He age of 6.44±0.12 Ma. This surface sample has a young, single-grain apatite He age of 5.85±0.12 Ma. A still younger (U–Th)/He age (4.14±0.08 Ma) has been determined for apatite from the P2 Porphyry in the deepest part of Bajo de la Alumbrera.

Collectively, our zircon He ages range from 6.8 to 5.1 Ma. Excluding a single outlier (6.55±0.26 Ma), most (U–Th)/He zircon ages range from 6.5 to 5.1 Ma, considerably younger than the U–Pb zircon ages of the associated porphyry intrusions. Scatter in these (U–Th)/He ages may be related to problems in the intracrystalline U–Th heterogeneity (Hourigan et al. 2005) and/or helium retention. Despite this, there is good agreement between the zircon He ages and the Ar data (e.g., low-temperature Ar diffusion appears to have occurred between 6.3 and 6.1 Ma in sample ACH9998), and these data provide evidence for low-temperature thermal events (or disturbance) younger than 6.5 Ma.

The apatite (U–Th)/He data, although for two single-grain analyses of two samples, are consistent with the dissipation of the thermal anomalies at Bajo de la Alumbrera by 4.0 Ma. We speculate that the difference in the apatite He ages may be influenced by diffusion and/or variations in cooling rates across the deposit. The youngest apatite He age (4.14±0.08 Ma) was obtained from deep within the deposit, whereas the higher-level samples records an older apatite He age (5.85±0.12 Ma).

Interpretation and discussion

All available chronologic data for the Bajo de la Alumbrera porphyry deposit are consistent with episodic magmatic–hydrothermal activity occurring during a period of two million years. Low-temperature thermochronology has revealed a longer than expected thermal history that persists up to one to two million years after the youngest dated intrusion in the deposit (Fig. 9). Comparison of different radioisotopic dating strategies (in this case, Ar- and He-

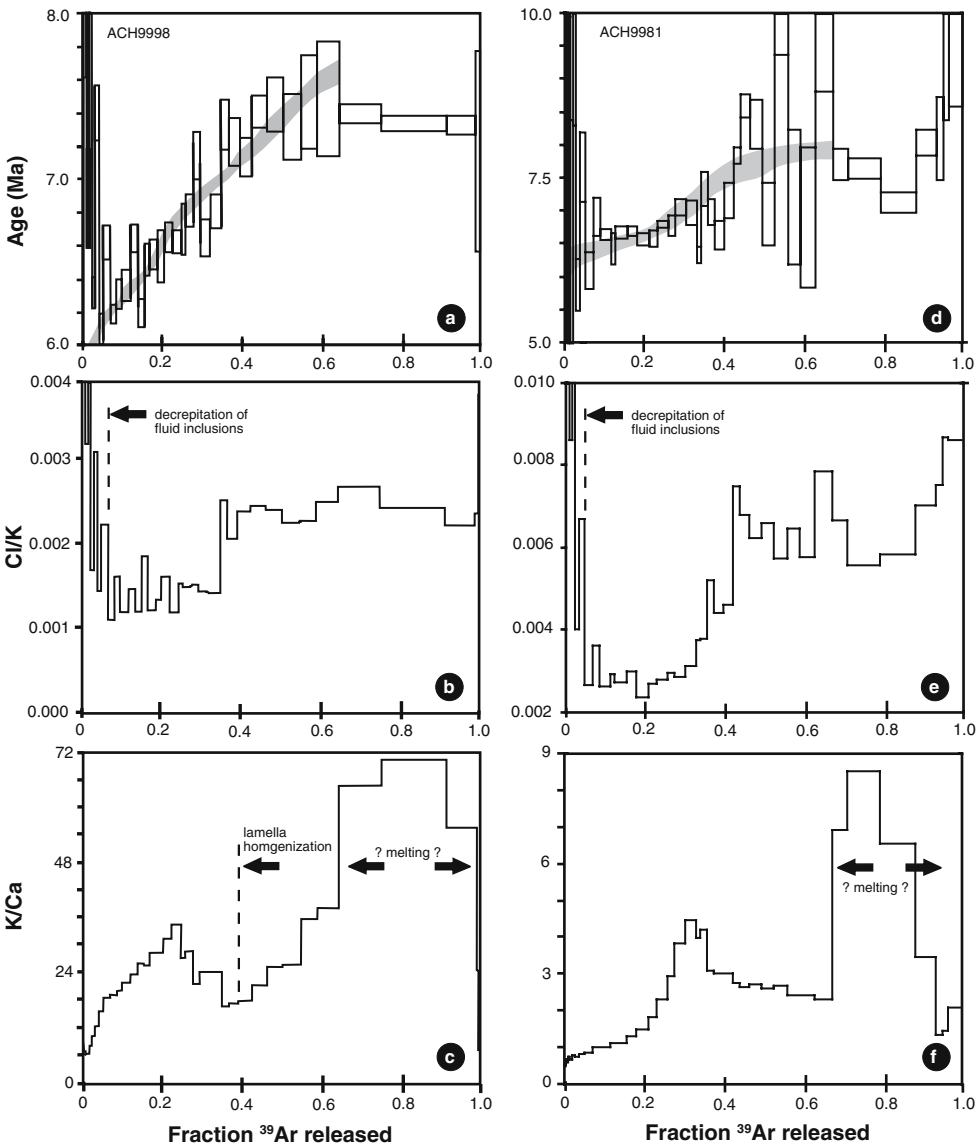

Fig. 8 **a, d** Laboratory-derived $^{40}Ar/^{39}Ar$ age spectrum for alkali feldspar phenocrysts from Late P3 Porphyry (Sample a ACH9998 and a ACH9981). Included is the multidiffuion domain model age spectrum (*gray line*). Note that model rises monotonically with increasing gas release (from *left* to *right*). **b, e** Calculated Cl/K ratios and **c, f** K/Ca ratios vs fraction of ^{39}Ar released for the alkali feldspar. See text for discussion

based) shows that low-temperature thermal events occurred outside the accepted period of cooling predicted via numerical simulations (Elder 1977; Norton and Cathles 1979; Cathles 1981; Norton 1982). For such events to happen, apparently disconnected from any known subsurface magma bodies, heat and/or volatiles must have been sourced from deeper-seated magma bodies or blind intrusions. Such findings have implications for the development of late-stage, low-temperature (illite-stable) hydrothermal alteration assemblages at Bajo de la Alumbrera.

Chronology of events

U–Pb zircon geochronology of Harris et al. (2004a) has shown that the mineralized porphyries at Bajo de la Alumbrera were emplaced during two main epochs (Fig. 10). The earliest (P2) mineralized porphyries were emplaced at about 8.0 Ma, whereas late-stage (Early and Late P3) porphyries were emplaced about a million years later (7.10±0.07; 6.96±0.09 Ma). By using multiple dating strategies on coexisting phases, it has been possible to show that these U–Pb zircon ages approximate the emplacement age of individual intrusions (cf. Halter et al. 2004). The unaltered Late P3 Porphyry has an undisturbed biotite $^{40}Ar/^{39}Ar$ age (7.15±0.18 Ma) that correlates well with the known U–Pb zircon age (6.96±0.09 Ma). The U–Pb zircon age for Late P3 Porphyry (7.10±0.07 and 6.96±0.09 Ma) overlap with Sasso's (1997) hornblende $^{40}Ar/^{39}Ar$ age determined for the postmineralization Northwest Porphyry (6.78±0.15 Ma). In other cases, apparently pristine phenocrystic biotite from the least-altered porphyry are poorly retentive of their argon (Harris et al. 2004a).

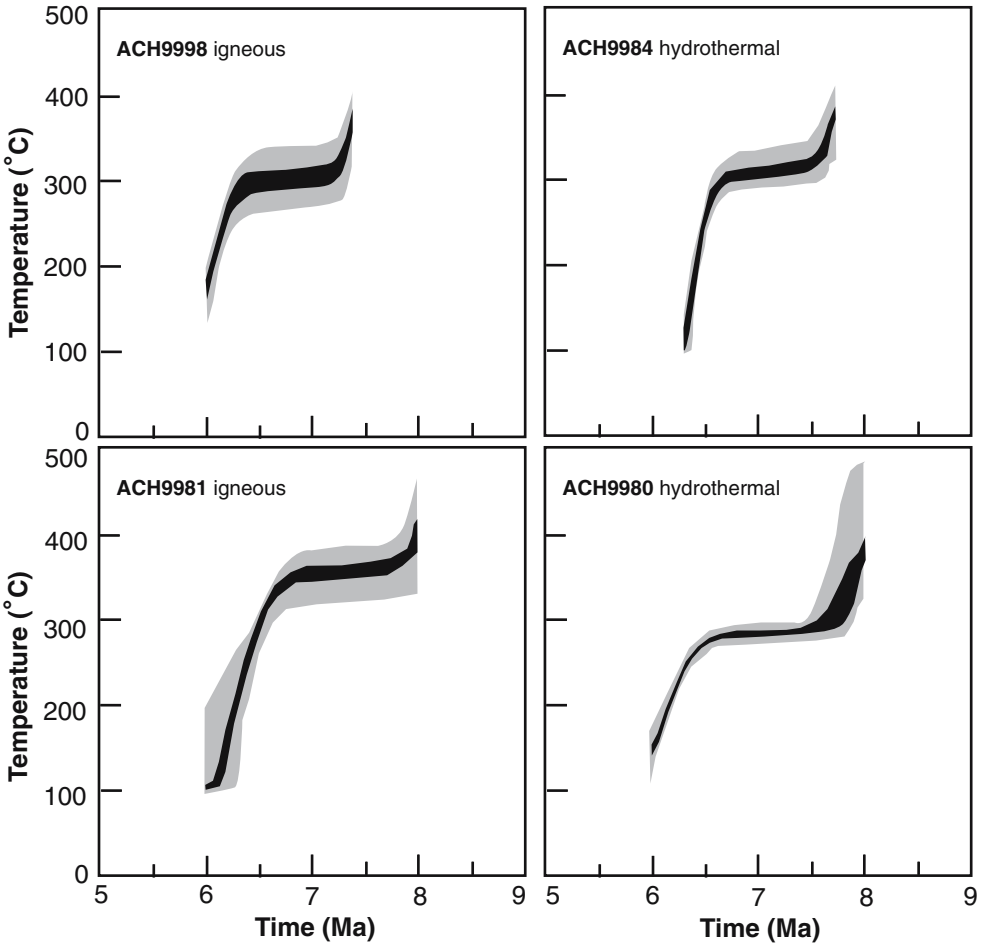

Fig. 9 Multidiffusion domain thermal modeling of alkali feldspar $^{40}Ar/^{39}Ar$ analyses. Model thermal histories for monotonic cooling (with confidence limits of 90% on the median of the population, *black*, and 90% confidence on distribution, *gray shading*) generated from the laboratory-derived Arrhenius data, using the computer programs of Lovera (available at http://sims.ess.ucla.edu/argon.html). Samples ACH9998 and ACH9981 are phenocrystic alkali feldspar from the Late P3 Porphyry. Samples ACH9980 and ACH9984 are hydrothermal alkali feldspar from the Early P3 Porphyry. Multidiffusion domain modeling shows that most samples cooled rapidly from magmatic temperatures to below about 300°C (between 6.6 and 6.4 Ma). Confidence is high for the portion of the model between 6.7 and 6.2 Ma, implicit in the reproducible model paths. This modeling suggests that most of the samples probably remained above 150°C until 6.0 Ma, if the monotonic cooling model is appropriate

Biotite total-fusion $^{40}Ar/^{39}Ar$ age determinations from altered porphyritic intrusions in the core of the Bajo de la Alumbrera deposit show that individual samples of altered biotite cooled through the biotite closure temperature (~ 300°C) at 7.10±0.13, 6.98±0.08, and 6.83±0.07 Ma (Sasso and Clark 1998). Our results confirm Sasso's biotite alteration ages; that is, assemblages overprinting the Early P3 Porphyry have an age of 7.12±0.13 Ma. For the P3 group of porphyries, our $^{40}Ar/^{39}Ar$ results show that the fluids associated with potassic assemblages cooled through the biotite closure temperature before 6.7 Ma. Still younger alkali feldspar ages (6.82±0.05 Ma and 6.64±0.09 Ma) suggest that fluid temperatures declined to below 300°C between 6.9 and 5.7 Ma.

The low-closure temperatures of K-rich minerals (<400°C) has meant that the precise age of potassic (biotite + K-feldspar) assemblages associated with P2 could not be determined. Secondary biotite from the P2 Porphyry (~8.0 Ma) yields one of the poorest spectra of this study (Fig. 5). The total-fusion age (7.08±0.95 Ma) of this biotite overlaps within uncertainty with the U–Pb ages of the P2 and P3 porphyries. The less precise nature of this biotite age appears to be a consequence of the postemplacement modification of early-formed alteration assemblages caused by hydrothermal fluids associated with the intrusion of the P3 group of porphyries. Despite field observations to the contrary (e.g., Proffett 2003), it appears that little to no relict age information remains that links the potassic alteration event to the P2 Porphyry.

Sasso and Clark (1998) determined a single $^{40}Ar/^{39}Ar$ whole rock age of 6.75±0.09 Ma for the phyllic (illite ± chlorite ± pyrite ± chalcopyrite ± quartz ± anhydrite) alteration assemblage. The porphyritic dyke sample that they analyzed has a complex alteration history. It was first altered to a potassic assemblage and was then replaced by illite ± chlorite, ultimately yielding a mixed age determination (Harris et al. 2004a). Based on the gas release history reported by Sasso (1997) and the nature of overprinting alteration assemblages, we infer this $^{40}Ar/^{39}Ar$ age to lie somewhere between that of potassic and late-stage phyllic alteration assemblage.

A number of lower-temperature (150–200°C) thermal events occurred after the emplacement of the porphyritic intrusions at Bajo de la Alumbrera. These have been constrained in part by our new (U–Th)/He ages (n=5). The (U–Th)/He results for magmatic zircon from P2 and P3 porphyries at Bajo de la Alumbrera yield a spread of ages between 6.8 and 5.1 Ma (Table 5, ESM). One zircon (U–

Th)/He age overlaps with the U–Pb zircon ages of the mineralized porphyritic intrusions; most range from 6.5 to 5.1 Ma. Based on estimated closure temperatures (Reiners et al. 2004), the single-grain (U–Th)/He zircon ages imply that the system last cooled through 180°C before 5.1 Ma. Young cooling ages (i.e., 5.9 and 6.6 Ma) are also implicit in the low-temperature degassing parts of the $^{40}Ar/^{39}Ar$ spectrum determined for alkali feldspars (both primary and secondary) in the P3 group of porphyries (see below).

The thermal collapse of the system most likely occurred before 4.0 Ma, based on our apatite (U–Th)/He age determinations (5.85±0.12 and 4.14±0.08 Ma; n=2). When considered together, the $^{40}Ar/^{39}Ar$ data and the zircon He and apatite He ages imply that either the Bajo de la Alumbrera system underwent protracted cooling over 4 million years or that one or more low temperature thermal events (increases in temperature to between 100 and 200°C) occurred one million years or more after the last known porphyritic intrusion was emplaced into the deposit.

Thermal modeling

To further evaluate the thermal history and test the idea that a low-temperature thermal pulse might have affected the rocks after about 6.9 Ma, we have undertaken thermal modeling using multidomain analysis (Lovera et al. 1989) of alkali feldspar (both igneous and hydrothermal) from several P3 porphyry samples. The analysis involved a $^{40}Ar/^{39}Ar$-stepwise degassing experiment in the laboratory, followed by numerical modeling of the gas release and inversion of the data to produce a model thermal history. The method of Lovera (1992) assumes that argon gas is released, under vacuum, by diffusion through naturally developed pathways and that the Arrhenius information obtained can be used to determine the kinetics of gas release. The kinetic information is used, in turn, to calculate model diffusion domains that are capable of matching the gas release from the stepwise degassing experiment performed in the laboratory (e.g., Lovera 1992). We then used a public domain modeling program (http://sims.ess.ucla.edu/argon.html) to invert the data into thermal histories of the monotonic cooling type.

Multidiffusion domain modeling of alkali feldspar data from this study are consistent with the samples cooling rapidly from magmatic temperatures to below about 300°C, probably soon after intrusion. As shown in Fig. 9, this is predicted to have occurred between 6.6 and 6.4 Ma. The portion of the model between 6.7 and 6.2 Ma is the best constrained for most of the samples, as indicated by the high confidence intervals implicit in the reproducible model paths (Fig. 9). Our modeling results suggest that most of the samples probably remained above 150°C until 6.0 Ma, if the monotonic cooling model is appropriate (Fig. 9). This prediction is supported by our (U–Th)/He study, whereby the majority of He data for bulk of the samples from the intrusions cluster between 6.4 and 5.1 Ma (n=4). This finding is comparable to other studies, wherein there is good correlation between (U–Th)/He and the $^{40}Ar/^{39}Ar$ data and whereby (U–Th)/He ages help to validate empirically the underlying assumptions of multi-domain diffusion modeling from alkali feldspar $^{40}Ar/^{39}Ar$ data (Reiners et al. 2004). Monotonic cooling models, combined with our (U–Th)/He ages, imply that the Bajo de la Alumbrera system cooled to 150°C between 6.0 and 5.1 Ma.

Correlation with Agua Rica

The Agua Rica porphyry deposit (1,714 Mt at 0.43% copper, 0.17 g/ton gold, 0.032% molybdenum; Perelló et al. 1998; Rojas et al. 1998; Landtwing et al. 2002) is located 25 km east of the central Farallón Negro district (Fig. 1). Porphyry-style mineralization has been overprinted by high-sulfidation alteration (Landtwing et al. 2002). Sasso and Clark (1998) reported an age of 6.29±0.04 Ma for secondary biotite at Agua Rica, whereas phyllic alteration has $^{40}Ar/^{39}Ar$ and K–Ar ages of 6.10±0.04 (Sasso and Clark 1998) and 5.38±0.05 Ma (Perelló et al. 1998), respectively. An $^{40}Ar/^{39}Ar$ age of 5.35±0.14 Ma (alunite) has been determined for the late-stage overprinting high-sulfidation epithermal alteration (Sasso and Clark 1998). Additional K–Ar ages of the epithermal alunite have been determined by Perelló et al. (1998), i.e., 6.18±0.05, 4.88±0.08, and 4.96±0.08 Ma. These results show that magmatism and hydrothermal alteration and mineralization occurred at Agua Rica between ~6.3 and 5.0 Ma. As such, magmatism at Agua Rica coincides with the suspected episode of thermal disturbance at Bajo de la Alumbrera. Therefore, evidence, albeit indirect, exists that suggest that the upper-crustal magma bodies that sourced the Agua Rica intrusions and mineralization were replenished at the same time that low-temperature thermal activity occurred at Bajo de la Alumbrera.

Summary

The Bajo de la Alumbrera deposit resulted from the superposition of multiple magmatic–hydrothermal systems. These were centered on two clusters of intrusions that were emplaced at ~8 and ~7 Ma (Harris et al. 2004a). Our new geochronologic data highlight the close temporal link of these intrusions to associated potassic alteration assem-

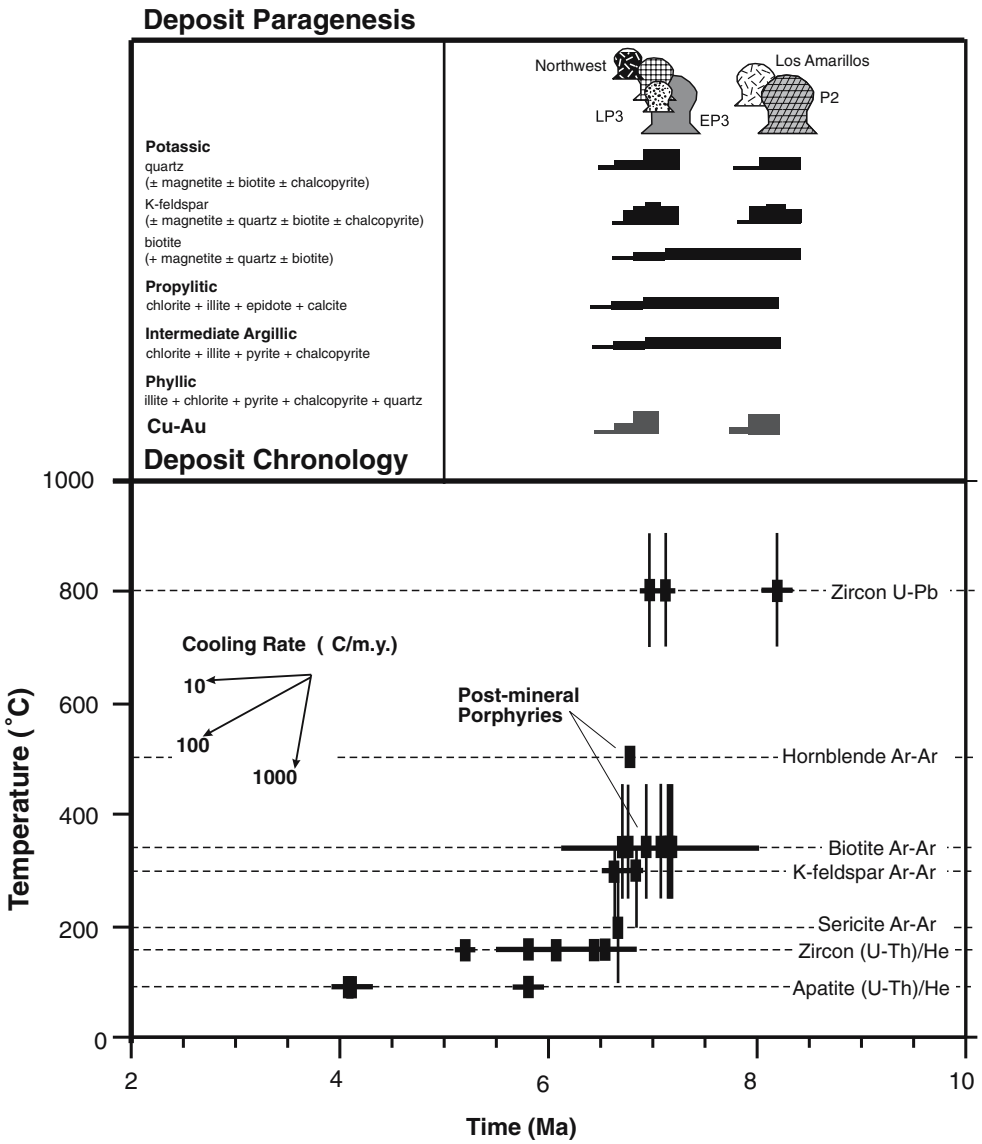

Fig. 10 Cooling history and paragenesis summary of the Bajo de la Alumbrera (Data sources: Sasso 1997; Sasso and Clark 1998; Harris et al. 2004a, b; new analytical results presented here). Also summarized here in the deposit paragenesis as reported by Proffett (2003) and modified by Harris et al. (2005). New (U–Th)/He data reveal that the magmatic–hydrothermal system cooled to approx. 200°C within 1.5 my of the last porphyry intrusion. Based on (U–Th)/He apatite data (with a closure temperature between 60 and 100°C), thermal collapse of the system occurred before 4 Ma (n=2). Thermal events associated with the emplacement of the P3 group of porphyries has reset the Ar systematics of alteration assemblages associated with the P2 porphyries

blages. Furthermore, our data (including modeling of available Ar-based geochronologic data) show that the system cooled below 150°C one million years or more after the emplacement of the last known intrusion in the Farallón Negro district (Fig. 10). Moreover, our $^{40}Ar/^{39}Ar$ and (U–Th)/He data reveals that these thermal perturbations (up to 200°C) were localized to the deposit.

Cooling of deep magma bodies of the size needed to produce porphyry ore deposits (10 s of cubic kilometers) occurs over periods of a million years without replenishment (e.g., Dilles and Wright 1988; Dilles and Einaudi 1992; Dalrymple et al. 1999; Hattori and Keith 2001). Although such magma bodies are commonly shown to evolve by open-system fractionation, magma mingling and incomplete mixing has been shown to be important in their evolution (e.g., Halter et al. 2004). For example, repeated influx of hydrous mafic magma would result in the sudden release of metal-rich magmatic volatiles (and melt). These volatiles can be transported to the site of ore deposition in compositionally evolved magmas to potentially form metal-rich hydrothermal alteration assemblages. Episodic replenishment is required to ensure the longevity of the magmatic system and/or its repeated reactivation beyond a million years. Without replenishment, crystallization of the source magma will occur, and fluid release will stop, leading to rapid cooling. During this thermal collapse, an external geothermal system invades the magmatic–hydrothermal system. Once this ingress of meteoric water occurs, numerical models predict that cessation of the system will result in less than 10,000 years (Norton 1982).

At Bajo de la Alumbrera, the bulk of the hydrothermal alteration was caused by repeated influx of magmatic volatiles, including the late-stage low-temperature (from 300 down to 150°C) phyllic assemblages (Ulrich et al.

2002; Harris et al. 2005). Independent modeling of stable isotope data suggests that above 200°C, the system was predominantly magmatic in origin, with dilution of the magmatic fluid system by meteoric water occurring after it had cooled through 200°C (Harris et al. 2005). All available thermochronometers confirm that Bajo de la Alumbrera last cooled below this temperature long after what is attributable to the thermal history of the high-level porphyries and/or their source magma body (Elder 1977; Norton and Cathles 1979; Cathles 1981; Norton 1982). To explain this chronologic data, new fluid-melt batches (supplying heat) must have been introduced late in the deposit's history (Fig. 10). It maybe that some late-stage low-temperature (~200°C) alteration assemblages developed in response to ascending magmatic fluids or via admixtures of magmatic–meteoric fluid circulated by a magmatic heat source. Our geochronologic and thermochronologic studies suggest that a magmatic–hydrothermal center can remain active or be reactivated over an extended period. Such findings are being increasingly reported (e.g., Barra et al. 2003; Maksaev et al. 2004; Masterman et al. 2004; Padilla-Garza et al. 2004; Deckart et al. 2005) and have implications for the timing of processes operating in underlying magma source regions to the higher crustal level porphyry ore deposits.

Acknowledgments The geologic mapping that forms the basis of this study was part of the first author's doctoral research at The University of Queensland, Brisbane. MIM Exploration (now Xstrata) and Minera Alumbrera are thanked for financial and logistical support and access to the Farallón Negro district. The first author would like to thank Stefan Nicolescu for analytical assistance on the (U–Th)/He ages and RSES for access to the ELA-ICP-MS, $^{40}Ar/^{39}Ar$, and mineral separation facilities. Thanks are also due to Rick Valenta, Steve Brown, John Proffett, David Keough, Rod Holcombe, Scott Bryan, Stephen Nano and Luis Rivera and the many others who have been involved with the project. The first author would like to thank the staff at the Australian Research Council Centre of Excellence in Ore Deposit Research, in particular Ross Large, for supporting this work. We also thank the Australian Nuclear Science and Technology Organisation and the Australian Institute for Nuclear Science and Engineering. The manuscript was improved significantly by the detailed reviews of Alan Clark, Mike Solomon, John Proffett, Jeremy Richards, and Victor Maksaev and discussions with James Cannell and Andrew Rae.

References

Allmendinger RW (1986) Tectonic development, southeastern border of the Puna Plateau, northwestern Argentine Andes. Geol Soc Am Bull 97:1070–1082

Arribas A Jr, Hedenquist JW, Itaya T, Okada T, Concepción RA, Garcia JS (1995) Contemporaneous formation of adjacent porphyry and epithermal Cu–Au deposits over 300 ka in northern Luzon, Philippines. Geology 23:337–340

Ballard JR, Palin JM, Williams IS, Campbell IH (2001) Two ages of porphyry intrusion resolved for the super-giant Chuquicamata copper deposit of northern Chile by ELA-ICP-MS and SHRIMP. Geology 29:383–386

Barra F, Ruiz J, Mathur R, Titley S (2003) A Re–Os study of sulfide minerals from the Bagdad porphyry Cu–Mo deposit, northern Arizona, USA. Miner Depos 38:585–596

Black LP, Kamo SL, Williams IS, Roudolis C, Claoué-Long JC, Korsch RJm, Davis DW (2000) The quest for a high-quality zircon standard for microbeam Pb–U–Th geochronology. Geol Soc Am Abstr Prog 59:43

Black LP, Kamo SL, Allen CM, Davis DW, Aleinikoff JN, Valley JW, Mundil R, Campbell IH, Korsch RJ, Williams IS, Foudoulis C (2004) Improved $^{206}Pb/^{238}U$ microprobe geochronology by the monitoring of a trace-element-related matrix effect; SHRIMP, ID-TIMS, ELA-ICP-MS and oxygen isotope documentation for a series of zircon standards. Chem Geol 205:115–140

Bossi GE, Muruaga CM, Sanagua JG, Hernado A, Ahumada AL (1993) Geologia y estratigrafia de la cuenca Neogena Santa Maria-Hualfin (Deptos. Santa Maria y Belen, Provincia de Catamarca: XII Congreso Geol. Argentino, v. Actas II, pp 156–165

Cathles LC (1981) Fluid flow and genesis of hydrothermal ore deposits. In: Skinner BJ (ed) Economic geology 75th anniversary volume. Society of Economic Geologists Publication, pp 424–457

Caelles JC, Clark AH, Farrar E, McBride SL, Quirt S (1971) Potassium–Argon ages of porphyry copper deposits and associated rocks in the Farallón Negro-Capillitas district. Catamarca, Argentina. Econ Geol 66:961–964

Cannell J, Cooke DR, Walshe JL, Stein H (2005) Geology, mineralization, alteration, and structural evolution of the El Teniente porphyry Cu–Mo deposit. Econ Geol 100:979–1003

Compston W, Williams IS, Meyer C (1984) U–Pb geochronology of zircons from lunar breccia 73217 using sensitive high mass-resolution ion microprobe. J Geophys Res 89(Suppl):B524–B525

Cornejo P, Tosdal RM, Mpodozis C, Tomlinson AJ, Rivera O, Fanning CM (1997) El Salvador, Chile porphyry Copper deposit revisited: geologic and geochronologic framework. Int Geol Rev 39:22–54

Coughlin TJ, O'Sullivan PB, Kohn BP, Holcombe RJ (1998) Apatite fission-track thermochronology of the Sierras Pampeanas, central western Argentina; implications for the mechanism of plateau uplift in the Andes. Geology 26:999–1002

Cumming GL, Richards JR (1975) Ore lead isotope ratios in a continuously changing earth. Earth Planet Sci Lett 28:155–171

Dalrymple GB, Grove M, Lovera OM, Harrison TM, Hulen JB, Lanphere MA (1999) Age and thermal history of the Geysers plutonic complex (felsite unit), Geysers geothermal field, California: a$^{40}Ar/^{39}Ar$ and U-Pb study. Earth and Planetary Science Letters v. 173 p. 285–298

Deckart K, Clark AH, Aguilar AC, Vargas RR, Bertens NA, Mortensen JK, Fanning M (2005) Magmatic and hydrothermal chronology of the giant Rio Blanco porphyry copper deposit, central Chile; implications of an integrated U–Pb and $^{40}Ar/^{39}Ar$ database. Econ Geol 100:905–934

Dilles JH, Einaudi MT (1992) Wall-rock alteration and hydrothermal flow paths about the Ann-Mason porphyry copper deposits, Nevada—a 6-km vertical reconstruction. Econ Geol 87:1963–2001

Dilles JH, Wright JE (1988) The chronology of Early Mesozoic Arc Magmatism in the Yerington district of western Nevada and its regional implication. Geological Society of America Bulletin v. 100 p. 644–652

Dilles JH, Einaudi MT, Gustafson LB (2000) Porphyry Cu–Mo–Au deposits; key research questions. Geol Soc Am Abstr Prog 32:2

Dunlap WJ, Kronenburg A (2001) Argon loss during deformation of micas: constraints from experimental deformation studies. Contrib Mineral Petrol 141:74–181

Elder JW (1977) Model of hydrothermal ore genesis: Volcanic Studies Group of the Geological Society of London, January 21–22, 1976, Proceedings, pp 4–13

Farley KA (2002) (U–Th)/He dating; techniques, calibrations, and applications. Rev Mineral Geochem 47:819–843

Farley KA, Wolf RA, Silver LT (1996) The effects of long alpha-stopping distances on (U–Th)/He ages. Geochim Cosmochim Acta 60:4223–4229

Foster DA, Harrison MT, Copeland P, Heizler TM (1990) Effects of excess argon within large diffusion domains on K-feldspar age spectra. Geochim Cosmochim Acta 54:1699–1708

González Bonorino F (1950) Geologia y petrografia de las hojas 12d (Capillitas) y 13d (Andalgalá): Buenos Aires Direccion Nacional de Geologia y Mineria, Boletin, 100 p

Gustafson LB, Orquera W, McWilliams M, Castro M, Olivares O, Rojas G, Maluenda J, Mendez M (2001) Multiple centers of mineralization in the Indio Muerto District, El Salvador, Chile. Econ Geol 96:325–350

Halter WE, Bain N, Becker K, Heinrich CA, Landtwing M, VonQuadt A, Clark AH, Sasso AM, Bissig T, Tosdal RM (2004) From andesitic volcanism to the formation of a porphyry Cu–Au mineralizing magma chamber: the Farallon Negro Volcanic Complex, northwestern Argentina. J Volcanol Geotherm Res 136:1–30

Harris AC, Allen CA, Bryan SE, Campbell IH, Holcombe RJ, Palin MJ (2004a) Measuring the longevity of regional volcanism hosting the Bajo de la Alumbrera Cu–Au deposit: implications for the genesis of porphyry ore deposits. Miner Depos 39:46–67

Harris AC, Kamenetsky VS, White NC, Steele DA (2004b) Volatile phase separation in silicic magmas at Bajo de la Alumbrera porphyry Cu–Au deposit, NW Argentina. Resour Geol 54:341–356

Harris AC, Golding SD, White NC (2005) The genesis of Bajo de la Alumbrera deposit: stable isotope evidence for a porphyry-related hydrothermal system dominated by magmatic aqueous fluids. Econ Geol 101:71–94

Harris AC, Bryan SE, Holcombe RJ (2006) Volcanic setting of the Bajo de la Alumbrera porphyry Cu-Au deposit, Farallon Negro Volcanics, Northwest Argentina. Economic Geology v. 101, p. 71–94

Harrison TM, Duncan I, McDougall I (1985) Diffusion of ^{40}Ar in biotite; temperature, pressure and compositional effects. Geochim Cosmochim Acta 49:2461–2468

Hattori KH, Keith JD (2001) Contribution of mafic melt to porphyry copper mineralization: evidence from Mount Pinatubo, Philippines, and Bingham Canyon, Utah, USA Mineralium Deposita v. 36 p. 799–806

Hedenquist JW, Richards JP (1998) The influence of geochemical techniques on the development of genetic models for porphyry copper deposits. In: Richards JP, Larson PB (eds) Techniques in hydrothermal ore deposits geology. Rev Econ Geol 10:235–256

Henry CD, Elson HB, Castor SB (1995) Brief duration of hydrothermal activity at Round Mountain, Nevada, determined from ^{40}Ar/^{39}Ar geochronology. Geol Soc Am Abstr Prog 27:A329

Hirata T, Nesbitt RW (1995) U–Pb isotope geochronology of zircon: evaluation of the laser probe-inductively coupled plasma mass spectrometry technique. Geochim Cosmochim Acta 59:2491–2500

Horn I, Rudnick RL, McDonough WE (2000) Precise elemental and istope ratio determination by simulataneous solution nebulatization and laser ablation ICP-MS: application to U–Pb geochronology. Chem Geol 164:281–301

Hourigan JK, Reiners PW, Brandon MT (2005) U–Th zonation-dependant alpha-ejection in (U–Th)/He chronometry. Geochim Cosmochim Acta 69:3349–3365

Jordan TE, Allmendinger RW (1986) The Sierras Pampeanas of Argentina: a modern analogue of Rocky Mountain foreland deformation. Am J Sci 286:737–764

Jordan TE, Zeitler P, Ramos V, Gleadow AJW (1989) Thermochronometruc data on the development of the basement peneplain in the Sierras Pampeanas, Argentina. J South Am Earth Sci 2:207–222

Kraemer B, Adelmann D, Alten M, Schnurr W, Erpenstein K, Kiefer E, van den Bogarrd P, Goerler K (1999) Incorporation of the Paleogene foreland into the Neogene Puna Plateau; the Salar de Antofalla area, NW Argentina. J South Am Earth Sci 12:157–182

Landtwing MR, Dillenbeck ED, Leake MH, Heinrich CA (2002) Evolution of the breccia-hosted porphyry Cu–Mo–Au deposit at Agua Rica, Argentina: progressive unroofing of a magmatic hydrothermal system. Econ Geol 97:1273–1292

Lanphere MA, Baadsgaard H (2001) Precise K–Ar, ^{40}Ar/^{39}Ar, Rb–Sr and U/Pb mineral ages from the 27.5 Ma Fish Canyon Tuff reference standard. Chem Geol 175:653–671

Lee JKW, Williams IS, Eillis DJ (1997) Pb. U. Th diffusion in natural zircon. Nature 390:159–162

Llambías EJ (1972) Estructura del grupo volcanico Farallón Negro, Catamarca, República Argentina. Rev Asoc Geol Argent 27:161–169

Lovera OM (1992) Computer programs to model ^{40}Ar/^{39}Ar diffusion data from multidomain samples. Comput Geosci 18:789–813

Lovera OM, Richter FM, Harrison TM (1989) The ^{40}Ar/^{39}Ar thermochronometry for slowly cooled samples having a distribution of diffusion domain sizes. J Geophys Res B Solid Earth Planets 94:17917–17935

Maksaev V, Munizaga F, McWilliams M, Fanning M, Mathur R, Ruiz J, Zentilli M (2004) New chronology for El Teniente, Chilean Andes, from U–Pb, ^{40}Ar/^{39}Ar, Re–Os, and fission-track dating: implications for the evolution of a supergiant porphyry Cu–Mo deposit. Soc Econ Geol Spec Publ 11:15–54

Marsh TM, Einaudi MT, McWilliams M (1997) ^{40}Ar/^{39}Ar geochronology of Cu–Au and Au–Ag mineralization in the Potrerillos district, Chile. Econ Geol 92:784–806

Masterman GJ, Cooke DR, Berry RF, Walshe JL, Lee AW, Clark AH (2004) Fluid chemistry, structural setting, and emplacement history of the Rosario Cu–Mo porphyry and Cu–Ag–Au epithermal veins, Collahuasi District, northern Chile. Econ Geol 100:835–862

Norton DL (1982) Fluid and heat transport phenomena typical of copper-bearing pluton environments; southeastern Arizona. In: Titley SR (ed) Advances in geology of porphyry copper deposits; southwestern North America. University of Arizona Press, Tucson, pp 59–73

Norton D, Cathles LM (1979) Thermal aspects of ore deposits. In: Barnes HL (ed) Geochemistry of hydrothermal ore deposits, 2nd edn. Wiley, New York, pp 611–631

Padilla-Garza RA, Titley SR, Eastoe CJ (2004) Hypogene evolution of the Escondida porphyry copper deposit, Chile. Soc Econ Geol Spec Publ 11:141–165

Pearce NJG, Perkins WT, Westgate JA, Gorton MP, Jackson SE, Neal CR, Chenery SP (1997) A complication of new and published major and trace element data for NIST SRM 610 and NIST SRM 612 glass reference materials. Geostand Newsl 21:115–144

Perelló J, Rojas N, Devaux C, Fava L, Etchart E, Harman P (1998) Discovery of the Agua Rica porphyry Cu–Mo–Au deposit, Catamarca province, northwestern Argentina. Part II. Geology. Australian Mineral Foundation Symposium Proceedings, pp 117–132

Proffett JM (1997) Geology of the Bajo de la Alumbrera porphyry Cu–Au deposits, Catamarca Province, Argentina. Minera Alumbrera Ltd., Internal Report

Proffett JM (2003) Geology of the Bajo de la Alumbrera porphyry copper–gold deposit, Argentina. Econ Geol 98:1535–1574

Ramos VA (1970) Estratigrafa y estructura del terciario en la Sierra de los Colorados (provincia de La Rioja), Republica Argentina. Rev Asoc Geol Argent 25:359–382

Ramos VA, Reynolds JH, Jordan TE, Tabbutt KD (1998) Time constraints for the uplift of the Sierras de Toro Negro, Umango, and Espinal, western Sierras Pampeanas, Argentina. Geol Soc Am Abstr Prog 20:61

Re GH (1995) Evolucion tectosedimentarua del depocentro de la cuenca del antepais andino (27°S–33°S) y su relacion con el cambio en el angulo de subduccion de la placa de Nazca: IX Congreso Latinoamericano de Geologia, Resumenes, Caracas, Venezuela, 1995, p 72

Renne PR, Swisher CC, Deino AL, Karner DB, Owens TL, DePaolo DJ (1998) Intercalibration of standards, absolute ages and uncertainties in $^{40}Ar/^{39}Ar$ dating. Chem Geol 145:117–152

Reynolds P, Ravenhurst C, Zentilli M, Lindsay D (1998) High-precision $^{40}Ar/^{39}Ar$ dating of two consecutive hydrothermal events in the Chuquicamata porphyry copper system, Chile. Chem Geol 148:45–60

Reiners PW, Ehlers TA, Garver JI, Mitchell SG, Montgomery DR, Vance JA, Nicolescu S (2002) Late Miocene exhumation and uplift of the Washington Cascade Range. Geology 30:767–770

Reiners PW, Zhou Z, Ehlers TA, Xu C, Brandon MT, Donelick RA, Nicolescu S (2003) Post-orogenic evolution of the Dabie Shan, eastern China, from (U–Th)/He and fission-track dating. Am J Sci 303:489–518

Reiners PW, Spell TL, Nicolescu S, Zanetti KA (2004) Zircon (U–Th)/He thermochronometry: He diffusion and comparisons with $^{40}Ar/^{39}Ar$ dating. Geochim Cosmochim Acta 68:1857–1887

Rojas, N, Perelló, J, Harman, P, Cabello, J, Devaux, C, Fava, L, Etchart, E (1998) Discovery of the Agua Rica porphyry Cu-Mo-Au deposit, Catamarca province, northwestern Argentina, Part I: Exploration and discovery: Australian Mineral Foundation Symposium, Perth, Western Australia, 30 November and 1 December 1998, Proceedings, p. 111–117.

Sasso AM (1997) Geological evolution and metallogenetic relationships of the Farallón Negro volcanic complex, NW Argentina: Ph.D. thesis, Queens University, 842 p

Sasso AM, Clark AH (1998) The Farallón Negro group, northwest Argentina: magmatic, hydrothermal and tectonic evolution and implications for Cu–Au metallogeny in the Andean back-arc. Soc Econ Geol Newsl 34:1, 8–18

Silberman ML, Bonham HF Jr, Garside LJ, Ashley RP (1979) Timing of hydrothermal alteration–mineralization and igneous activity in the Tonopah mining district and vicinity, Nye and Esmeralda Counties, Nevada. Nevada Bureau Mines Geol Rep 33:119–126

Sister RG (1963) Informe geológico–económico de Farallón Negro y zona adyacente, Distrito Haulfin, Departamento Belen, Provincia de Catamarca, Opera Lilloana, VIII, 164 p

Spell TL, McDougall I (2003) Characterization and calibration of $^{40}Ar/^{39}Ar$ dating standards. Chem Geol 198:189–211

Tosdal RM, Richards JP (2001) Magmatic and structural controls on the development of porphyry Cu±Mo±Au deposits. Rev Econ Geol 14:157–181

Ulrich T, Heinrich CA (2002) Geology and alteration geochemistry of the porphyry Cu–Au deposit at Bajo de la Alumbrera, Argentina. Econ Geol 96:1719–1742

Ulrich T, Günthur D, Heinrich CA (2002) The evolution of a porphyry Cu–Au deposit, based on LA-ICP-MS analysis of fluid inclusions: Bajo de la Alumbrera, Argentina. Econ Geol 96:1743–1774

Vandervoort DS, Jordan TE, Zeitler PK, Alonso RN (1995) Chronology of internal drainage development and uplift, southern Puna Plateau, Argentine Central Andes. Geology 23:145–148

Villeneuve M, Sandeman HA, Davis WJ (2000) A method for intercalibration of U–Th–Pb and ^{40}Ar–^{39}Ar ages in the Phanerozoic. Geochim Cosmochim Acta 64:4017–4030